The Chromium-Nickel-Carbon (Cr-Ni-C) Phase Diagram

T.Ya. Velikanova, A.A. Bondar, and A.V. Grytsiv

(Submitted 27 March 1998; in revised form 30 September 1998)

Phase equilibria of the Cr-Ni-C system in the melting (crystallization) range were investigated by means of metallography, microprobe analysis, powder x-ray diffraction, differential thermal analysis, and melting point technique (Pirani and Alterthum method). On the basis of received results and assessment of available literary data, the phase diagram was presented as projections of solidus, liquidus, and melting (crystallization) diagram, reaction scheme at crystallization (melting), a number of vertical and isothermal sections. No ternary compounds were found in the system. The Ni-base phase forms equilibria with all others. The character of solid-phase equilibria does not change in the temperature range under investigation, from solidus to 800 °C.

1. Introduction

A number of investigations of Cr-Ni-C alloys have been made prior to the beginning of the work described in this article. These investigations include experimental work relevant to the phase diagram of the system [40Mur, 55Kos, 71Tel, 74Lob, 75Tum, 81Ale, 82Tum]. and thermodynamic simulations of the phase equilibria of the system [81Guz, 90Kaj]. In the published experimental work are isothermal sections at 800 °C [55Kos], 1000 °C [82Tum], 1100 °C [71Tel, 82Tum], and 1200 °C [82Tum], projections of liquidus surface [40Mur, 55Kos], and vertical sections through the C isoconcentrates [40Mur], 0.5, 1.8, 4, and 6.5 mass%. All these data have been represented in [95Vil] without any criticism. The joint solubility of Cr and C in Ni has also been investigated in [74Lob], [75Tum], [81Ale], and [82Tum].

Despite the extensive number of published papers, information on the Cr-Ni-C system remained incomplete and inadequate for definition of a complete phase diagram. Indeed, in some cases the data were contradictory. The isothermal sections of [82Tum] at 1000, 1100, and 1200 °C were plotted on the basis of research in a narrow concentration interval near the homogeneity field of the Ni solid solution. In the works of [74Lob], [75Tum], and [82Tum], seven binary Cr-Ni alloys (5-26 mass% Cr) were carbonized under a hydrogen and methane mixture at 700 to 1200 °C; the carbonization was followed by a study of C activity and phase boundaries (the latter by metallographic and x-ray diffraction, XRD, techniques). Analogous research was carried out at 1000 °C by [81Ale] with nine alloys in the range 0 to 30 at.% Cr. Phase equilibria at 1100 °C were investigated by [71Tel] solely by powder XRD with an insignificant number of alloys (13 compositions). In contrast, [55Kos] investigated 90 alloys in detail by metallography, powder XRD, and thermal analysis. The data of [40Mur] and [55Kos] on invariant equilibria in the melting range differ considerably in temperature results. It is possible that the lower values of [55Kos] could be explained by their determination of melting temperatures with cooling curves and that supercooling was responsible for their low values.

In order to understand and forecast properties of the industrial chromium carbide-nickel alloys, the data on coordinates of invariant equilibria are of prime importance. The authors' analysis [93Bon] showed that even insignificant errors in this data could result in essential mistakes of interpretation of structure/property dependencies. So, the authors have repeatedly investigated the phase equilibria of this system by measurements of alloy melting and constructed the entire phase diagram by combination of their experimental results with literature data.

T.Ya. Velikanova, A.A. Bondar, and **A.V. Grytsiv,** I.N. Frantsevich Institute for Problems of Materials Science, National Academy of Science of Ukraine, 252180, Krzhyzhanovskogo str. 3, Kyiv, Ukraine.

2. Binary Reference Systems

Crystal data for the elemental phases and the chromium carbides are given in Table 1. The binary Ni-C and Ni-Cr systems from [90Mas], where the Ni-C system is taken from [89Sin] and the Ni-Cr system from [86Nas] and [91Nas], were accepted for this investigation. For the Cr-C system, the higher temperatures of the invariant equilibria observed in earlier work by the present authors [87Yer] are preferred to those of the diagram in [90Mas], which is taken from [90Ven] and based on the work of [69Rud]. Accordingly, the data of [87Yer] were accepted.

Table 1 Crystal structure phases

Phase	Sign	Pearson symbol	Space group	Prototype	Lattice parameters, pm		
					a	*b*	*c*
(Cr)	(Cr)	*cI*2	$Im\bar{3}m$	W	288.44	…	…
(Ni)	(Ni)	*cF*4	$Fm\bar{3}m$	Cu	352.38	…	…
C	C	*hP*4	$P6_3$	C (graphite)	246.4 ± 0.2	…	671.1 ± 0.4
($Cr_{23}C_6$)	φ	*cF*112	$Fm\bar{3}m$	$Cr_{23}C_6$	1065.0 ± 0.2	…	…
(Cr_7C_3)	ϑ	*hP*80	*P*3*c*1	Cr_7C_3	140.1	…	453
(Cr_3C_2)	τ	*oP*20	*Pnma*	Cr_3C_2	553.29 ± 0.05	282.90 ± 0.02	1147.19 ± 0.07

Source: [90Mas] and [91Vil]

Table 2 Solidus temperature after Pirani-Alterthum method, thermal treatment and phase compositions (XRD and metallography) for the Cr-Ni-C alloys

Composition, at.%		Temperature of solidus, °C					Thermal treatment		Phase composition
Cr	C	t_{opt}(a)	t_{act}(a)	$\pm\Delta_{st}$(a)	$\pm\Delta_{tot}$(a)	*n*	t_{an}(b)	τ(b), min	
80	10	1434	1442	6	7	5	1410	50	(Cr) + φ
66	10	1301	1308	1	4	5	1300	50	(Cr) + (Ni) + φ
65	20	1304	1310	1	4	5	1300	50	(Ni) + φ + ϑ
59	18	1304	1310	5	6	4	1290	45	(Ni) + φ + ϑ
56	10	1315	1324	6	7	5	1305	55	(Ni) + φ + ϑ
54	10	1310	1316	1	4	5	1300	55	(Ni) + φ + ϑ
45	10	1309	1316	3	6	4	1305	60	(Ni) + ϑ
40	10	1312	1324	5	6	6	1285	50	(Ni) + ϑ
39	10	1303	1316	2	4	4	1295	45	(Ni) + ϑ
38	10	1306	1318	3	4	3	1300	55	(Ni) + ϑ
36	10	1305	1312	2	4	5	1290	40	(Ni) + ϑ
34	10	1300	1307	3	5	5	1275	55	(Ni) + ϑ
32.5	10	1284	1290	2	4	5	1280	55	(Ni) + ϑ
31.5	10	1278	1285	3	5	5	1265	50	(Ni) + ϑ
46	25	1242	1252	3	5	5	1230	50	(Ni) + ϑ + τ
27	10	1254	1261	4	6	4	1245	50	(Ni) + ϑ + τ
24	10	1246	1257	3	5	4	1235	60	(Ni) + τ
23	10	1249	1256	2	5	4	1245	70	(Ni) + τ
29	25	1235	1246	2	4	4	1195	45	(Ni) + τ + C
18	10	1229	1240	12	13	4	1215	45	(Ni) + τ + C
13	10	1265	1269	24	24	3	1140	45	(Ni) + τ + C
3	10	1313	1319	6	7	2	1300	45	(Ni) + C
0	90	1317	1329	2	4	3	1315	25	(Ni) + C
56	0	1333	1345	5	6	5	1320	55	(Cr) + (Ni)

(a) t_{opt} and t_{act} stand for optical and actual temperatures of solidus, Δ_{st} and Δ_{tot} are statistical and total errors (95 % confidence limits), *n* is the number of measurements.
(b) t_{an} means annealing temperature, t is the total duration of expose time at subsolidus temperature during measurements.

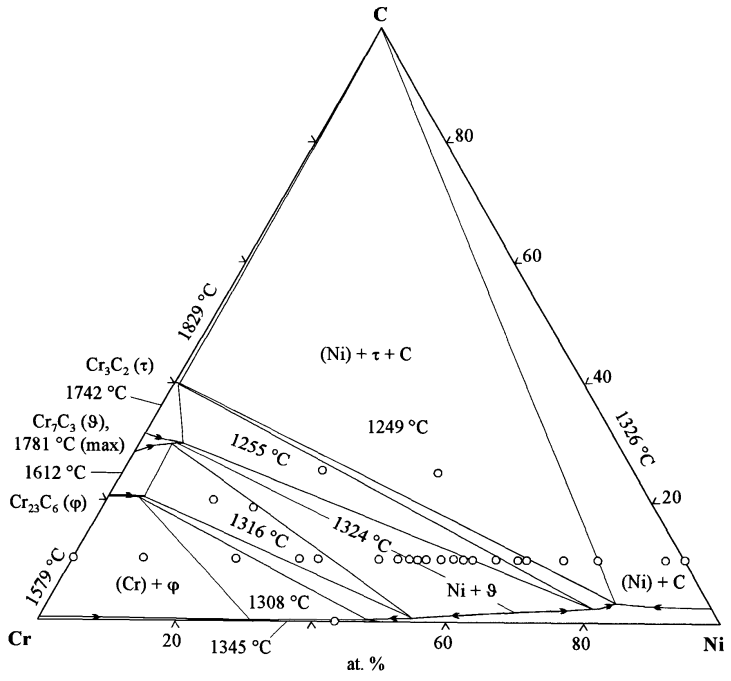

Fig. 1 Projection of solidus surface of the Cr-Ni-C system. Circles show the composition of investigated alloys.

3. Experimental Details

3.1 Alloy Preparation

The starting materials for this investigation (all in mass%) were: Cr, 99.9%; Ni, >99.5%; and nuclear graphite with 0.05% ash, 0.023% S, and <0.02% Fe. Master alloys—$Ni_{90}C_{10}$, $Cr_{90}C_{10}$, and $Cr_{59.3}C_{40.7}$—were first prepared from the elemental materials under the same conditions as was later used for preparing ternary alloys. The compositions of the master alloys were carefully established by chemical analysis. Ternary alloys of 23 compositions (Fig. 1 and Table 2) were prepared from these master alloys by arc melting with a nonconsumable tungsten electrode on a water-cooled Cu hearth under an argon atmosphere (pressure ~80 kPa) that had previously been gettered by melting Ti for 3 min. Mixtures of 10 or 15 g mass were sintered with a weak arc and then melted twice with inversion between meltings to achieve homogenization. The ingots were then crushed and remelted in the same way. The total weight losses on melting were always less than 0.5 mass%; therefore, the alloys were not chemically analyzed, but nominal compositions were adopted.

3.2 Experimental Methods

As-cast alloys and alloys annealed at subsolidus temperatures were investigated by metallography, electron probe microanalysis (EPMA), and XRD. Standard polishing, etching, and optical microscopic techniques were used when preparing polished samples. Scanning electron microscopy and EPMA were done with a JEOL Superprobe 733 (Japan) instrument. Because the errors in determining C content considerably exceed the errors in determining Cr and Ni contents, metal ratios were measured for coexisting phases and eutectics.

X-ray diffraction was performed using filtered Cr Kα and Cu Kα radiation. Debye-Scherrer patterns of powder specimens were taken with a 57.3 mm diameter camera. After film shrinkage correction, data from the diffraction maxima were put into the authors' weighted least-squares program, which is based largely on the algorithm of [51Hes]. This program provides lattice parameters with 95% confidence limits.

Phase transformations up to liquidus temperatures were examined by differential thermal analysis (DTA) under high-purity helium with samples in alundum crucibles. Measurements were in an apparatus with a string thermocouple design [71Koc]; this design reduces contact between thermocouple and ceramic. Runs were made with a rate of temperature change near 60 °C/min. The W/W-Re 20 thermocouple (80 mass% W, 20 mass% Re) was calibrated against the IPTS-90 reference points of Al, Au, Pd, Pt, Rh, plus additional points for Fe and Si.

Solidus temperatures (Table 2) were determined by the Pirani and Alterthum method of [23Pir]. Bar-shaped specimens, which were clamped between two water-cooled Cu electrodes through W inserts, were heated resistively under high-purity helium near atmospheric pressure. Temperature was measured with a disappearing filament optical pyrometer focused on a blackbody hole having a diameter-to-depth ratio of 1 to 4. The maximum instrumental error amounted to ±2.8 °C at 900 to 1400 °C. Melting temperature was determined when the character of optical reflection changed due to the fusion-induced change of shape at the bottom of the hole [65Yer], which is observed as formation of a black spot. Three to five melting determinations were made on each sample. The durations of sample subsolidus exposure during melting determinations were 10 to 50 min. After melting measurement, samples were annealed 10 to 30 °C below the solidus for 30 min and then quenched at a rate of 200 to 300 °C/s.

Optical (brightness) temperature (T_1/K) is underestimated in comparison to true temperature (T_o/K) during optical pyrometric measurements because of two factors: (1) absorption of radiation by the viewing window and (2) nonblackbody conditions. Correction of the optical temperature can be made with the following formula:

$$\left(\frac{1}{T_o}\right) = \left(\frac{1}{T_1}\right) + A \qquad \text{(Eq 1)}$$

Here A is the correction factor and is the sum of two terms. The first is the absorption correction for the 2 mm thick viewing window. This correction was established experimentally in much the same manner as described by [67Rud] and was found to be $A_1 = -(3.7 \pm 0.5) \times 10^{-6}$/K. The second correction for nonblackbody conditions is evaluated from the formula, $A_2 = (\lambda/C) \ln \varepsilon_{0.65}$, where the wavelength $\lambda = 0.65$ μm, $C = 14{,}388$ μm · K, and $\varepsilon_{0.65}$ denotes the emissivity coefficient of the given blackbody hole. The value of the emissivity coefficient depends on the diameter-to-depth ratio and the emissivity coefficient of the material being tested. Data from [64Lis] were used to evaluate this term with the unknown emissivity coefficients of Cr-Ni-C alloys being crudely approximated as an additive sum of the emissivity coefficients of the component elements weighted on the basis of atomic fractions. The total accumulated errors in the temperature measurements with the Pirani-Alterthum method were estimated to a 95% confidence limit as a combination of random (statistical) errors, instrumental errors of the pyrometer and ammeter, and errors in the corrections.

Comparison of Pirani-Alterthum (Table 2) and DTA (Table 3) solidus temperatures shows generally good agreement. The corrected temperatures of the Pirani-Alterthum measurements were accepted in preference to the DTA values. This preference is due to the fact that a number of factors affect DTA measurements that could not be evaluated; these include purity of the reference specimens, in situ contamination, instrumental errors, and so forth. It may be noted that the temperatures from the Pirani-Alterthum technique coincide quite well with reported values for the invariant equilibria of the binary Cr-Ni and Ni-C systems.

4. Results and Discussion

Experimental results (Tables 2 through 6) form the basis for construction of the phase diagram as projections of solidus, liquidus surfaces, and melting (crystallization) diagrams (Fig. 1-3), reaction scheme (Fig. 4), and a number of vertical sections (Fig. 5-7).

Table 3 Phase transformation temperature of alloys after DTA

Composition, at.%		Temperature of thermal arrest at heating, °C	Phase transformation at heating (…/…) or invariant equilibria (… ↔ …)	Maximum temperature of heating, °C
Cr	C			
80	10	1420	(Cr) + φ/L + (Cr) + φ	1557
		1529	L + (Cr) + φ/L + (Cr)	
66	10	1328	L ↔ (Cr) + (Ni) + φ	1422
		1404	L + φ/L	
65	20	1336	L + ϑ ↔ (Ni) + φ	1400
59	18	1332	L + ϑ ↔ (Ni) + φ	1410
56	10	1329	L + ϑ ↔ (Ni) + φ	1428
		1404	L + ϑ/L	
54	10	1338	L + ϑ ↔ (Ni) + φ	1400
45	10	1334	(Ni) + ϑ /L + (Ni) + ϑ	1404
42	10	1339	(Ni) + ϑ /L + (Ni) + ϑ	1430
40	10	1340	L ↔ (Ni) + ϑ	1400
		1358	L + ϑ/L	
39	10	1339	(Ni) + ϑ/L + (Ni) + ϑ	1412
38	10	1340	(Ni) + ϑ/L + (Ni) + ϑ	1430
		1381	L + ϑ/L	
36	10	1328	(Ni) + ϑ/L + (Ni) + ϑ	1400
		1360	L + ϑ/L	
34	10	1316	(Ni) + ϑ/L + (Ni) + ϑ	1400
		1355	L + ϑ/L	
32.5	10	1291	(Ni) + ϑ/L + (Ni) + ϑ	1335
46	25	1267	L + ϑ ↔ (Ni) + τ	1333
27	10	1267	L + ϑ ↔ (Ni) + τ	1400
		1283	L + (Ni) + ϑ/ L + (Ni)	
		1330	L + (Ni)/L	
23	10	1253	(Ni) + τ/L + (Ni) + τ	1380
		1331	L + (Ni)/L	
29	25	1236	L ↔ (Ni) + τ + C	1380
		1280	L + τ + C/L + C	
18	10	1241	L ↔ (Ni) + τ + C	1342
		1281	L + (Ni)/L	
13	10	1232	L ↔ (Ni) + τ + C	1380
		1287	L + (Ni) + C/L + (Ni)	
		1329	L + (Ni)/L	
3	10	1311	(Ni) + C/L + (Ni) + C	1358
		1356	L + C/L	
0	90	1340	L ↔ (Ni) + C	1400
56	0	1318	L ↔ (Cr) + (Ni)	1356

4.1 Solidus Surface

Tables 4 and 5 show ternary compounds to be absent in the system. Chromium carbides are confirmed to be in equilibria with (Ni) and (Cr) solid-solution phases to form two- and three-phase regions on the solidus surface (Fig. 1). Microstructures of alloys from three-phase regions are shown in Fig. 8(a) to (h). Comparison of structures for as-cast alloys and alloys annealed at subsolidus temperatures shows that annealing produces integration of structure with thin-phase boundaries, which verifies the attainment of equilibrium. X-ray diffraction patterns of annealed samples contain narrow reflections and are split into doublets at high angles by α_1,α_2 resolution. Because the annealing temperatures were very close to the solidus (Table 2), the authors considered the microstructures and XRD patterns to be representative of the state on the solidus surface. The metal content ratios of phases coexisting in three-phase equilibria at the solidus were determined by EPMA (Table 6). The combination of EPMA, XRD, and metallographic data, and solidus temperatures allowed the determination of the positions of the three-phase boundaries and their phase compositions. One can see that the terminal solid solutions of (fcc Ni) and (bcc Cr) have ranges of homogeneity greater than any of the other solid phases.

Carbon solubilities in the metal phases were estimated by the authors on the basis of literature data with consideration of their results concerning location of phase boundaries. The maximum C solubility in (Ni) is based on the work of [81Ale] and [82Tum] and occurs at the point of contact with the three-phase (Ni) + (Cr_3C_2) + C field. Figure 9(a) to (d) gives the composition-temperature dependencies to this Ni apex of the

Table 4 Lattice parameters for the Cr-Ni-C alloys annealed at subsolidus temperatures

Composition, at.%		Phase		Lattice parameters, pm		
Cr	C	composition	Phase	*a*	*b*	*c*
80	10	(Cr) + φ	(Cr)	288.2 ± 0.5	…	…
			φ	1070 ± 2	…	…
66	10	(Cr) + (Ni) + φ	(Ni)	359.8 ± 0.1	…	…
			(Cr)	286.5 ± 0.2	…	…
			φ	1064.7 ± 0.7	…	…
56	10	(Ni) + φ + ϑ	(Ni)	357.8 ± 0.3	…	…
			φ	1064.3 ± 0.3	…	…
			ϑ	(Trace)	…	…
45	10	(Ni) + ϑ	(Ni)	357.1 ± 0.2	…	…
			ϑ	1405 ± 2	…	451 ± 2
40	10	(Ni) + ϑ	(Ni)	356.1 ± 0.1	…	…
			ϑ	1402.4 ± 0.5	…	451.9 ± 0.5
38	10	(Ni) + ϑ	(Ni)	355.9 ± 0.3	…	…
			ϑ	1404.6 ± 0.5		452.0 ± 0.5
36	10	(Ni) + ϑ	(Ni)	355.9 ± 0.4	…	…
			ϑ	1399.3 ± 0.3	…	450.9 ± 0.3
34	10	(Ni) + ϑ	(Ni)	355.71 ± 0.09	…	…
			ϑ	(Trace)	…	…
32.5	10	(Ni) + ϑ	(Ni)	355.2 ± 0.1	…	…
			ϑ	(Trace)	…	…
31.5	10	(Ni) + ϑ	(Ni)	354.94 ± 0.09	…	…
			ϑ	1400 ± 2	…	449 ± 8
46	25	(Ni) + ϑ + τ	(Ni)	355 ± 2	…	…
			ϑ	1401 ± 2	…	448 ± 2
			τ	554.4 ± 0.5	283.1 ± 0.6	1146 ± 2
27	10	(Ni) + ϑ + τ	(Ni)	355.0 ± 0.3	…	…
			ϑ	(Trace)	…	…
			τ	(Trace)	…	…
23	10	(Ni) + τ	(Ni)	354.9 ± 0.3	…	…
			τ	(Trace)	…	…
29	25	(Ni) + τ + C(a)	(Ni)	354.69 ± 0.09	…	…
			τ	553.7 ± 0.5	283.1 ± 0.5	1148 ± 2
13	10	(Ni) + τ + C(a)	(Ni)	355.1 ± 0.2	…	…
			τ	(Trace)	…	…
3	10	(Ni) + C(a)	(Ni)	353.49 ± 0.08	…	…
0	90	(Ni) + C(a)	(Ni)	353.23 ± 0.04	…	…
56	0	(Cr) + (Ni)	(Ni)	361.2 ± 0.2	…	…
			(Cr)	285.5 ± 0.5	…	…

(a) Phase was not detected by XRD.

tie triangle as well as for the point of contact with the (Ni) + (Cr_7C_3) + (Cr_3C_2) three-phase region. For the (Ni) + (Cr_3C_2) + C contact, the data of [55Kos] and [82Tum] are in good agreement with this work and are a satisfactory representation of the solvus curve (Fig. 9a and b); the work of [81Ale] undervalues the Cr and C content. For the (Ni) + (Cr_7C_3) + (Cr_3C_2) contact (Fig. 9c and d), the temperature dependence of the Cr content of [82Tum] extrapolates the authors' value at the solidus, but data of [82Tum] for C content extrapolate to a value much lower than that of the present investigation. In contrast, the C content found by [55Kos] seems high at lower temperatures, but is in quite reasonable agreement near the solidus temperature.

Maximum solubility of C in (Ni) reaches about 3 at.% C at 13.6 at.% Cr and decreases with further increase in Cr content. The C content in (Ni) at the point of contact with the (Cr) + ($Cr_{23}C_6$) + (Ni) phase field amounts to ~0.5 at.% C at the solidus temperature. Carbon solubility for the (Cr) phase in the ternary system was not investigated. At the solidus temperature it should not exceed the maximum solubility in the binary Cr-C system, which is ~0.4 at.%; this value results from extrapolation of data from [77Pou] and [85Pou].

At small Cr content, the (Ni) lattice parameter of the ternary solid solution is larger than the parameter of binary solid solutions at equivalent C contents. As the Cr content increases, the difference between these lattice parameters gradually decreases, indicating that the terminal solubility of C in (Ni) decreases with Cr content at higher Cr concentrations.

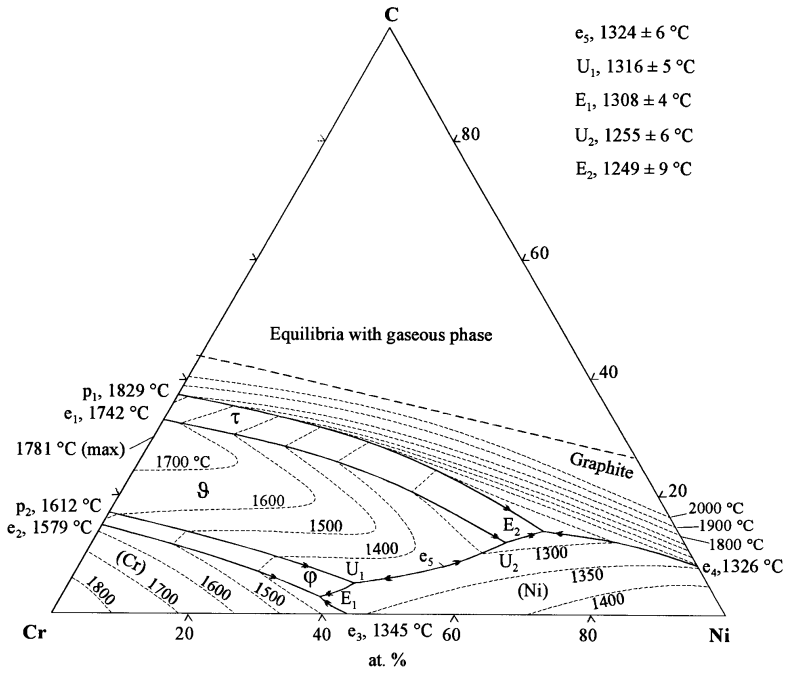

Fig. 2 Projection of liquidus surface of the Cr-Ni-C system

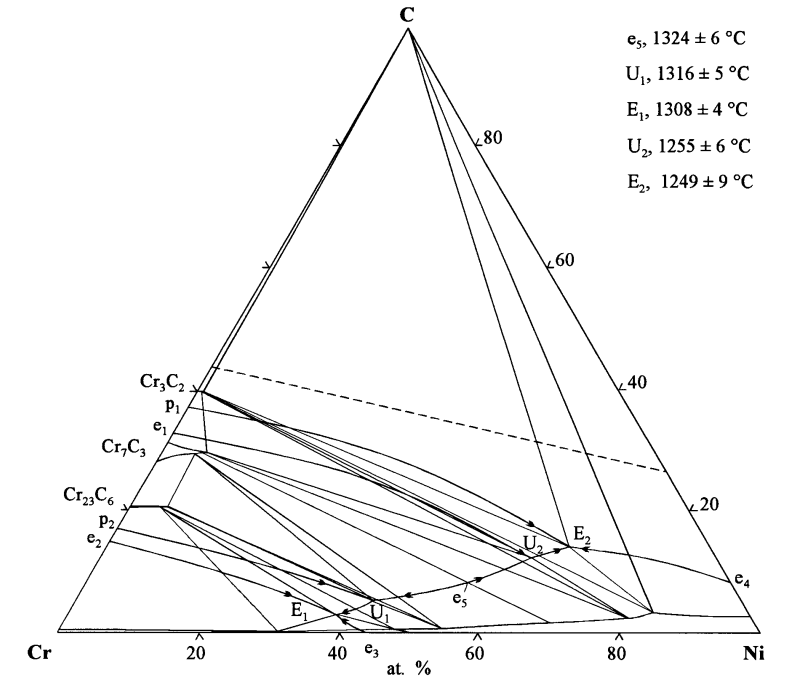

Fig. 3 Projection of the Cr-Ni-C phase diagram at melting (crystallization) of alloys on the concentration triangle

Electron probe microanalysis data indicate maximum solid solubility of Ni in chromium carbides to be 5 at.% for ($Cr_{23}C_6$), 6 at. % for (Cr_7C_3), and 0.7 at.% for (Cr_3C_2). These results at solidus temperatures are close to the values of [55Kos] for 800 °C and of [71Tel] for 1100°C, which indicates an obviously weak temperature dependence for the Ni solubilities in chromium carbides. The lattice parameters of the chromium carbides containing Ni do not differ appreciably from those of the binary carbides (compare Tables 1 and 7; see Fig. 10). This is reasonable because the atomic radii of Cr and Ni are closely comparable and the solubility of Ni in these carbides is low.

(text continued on p 140)

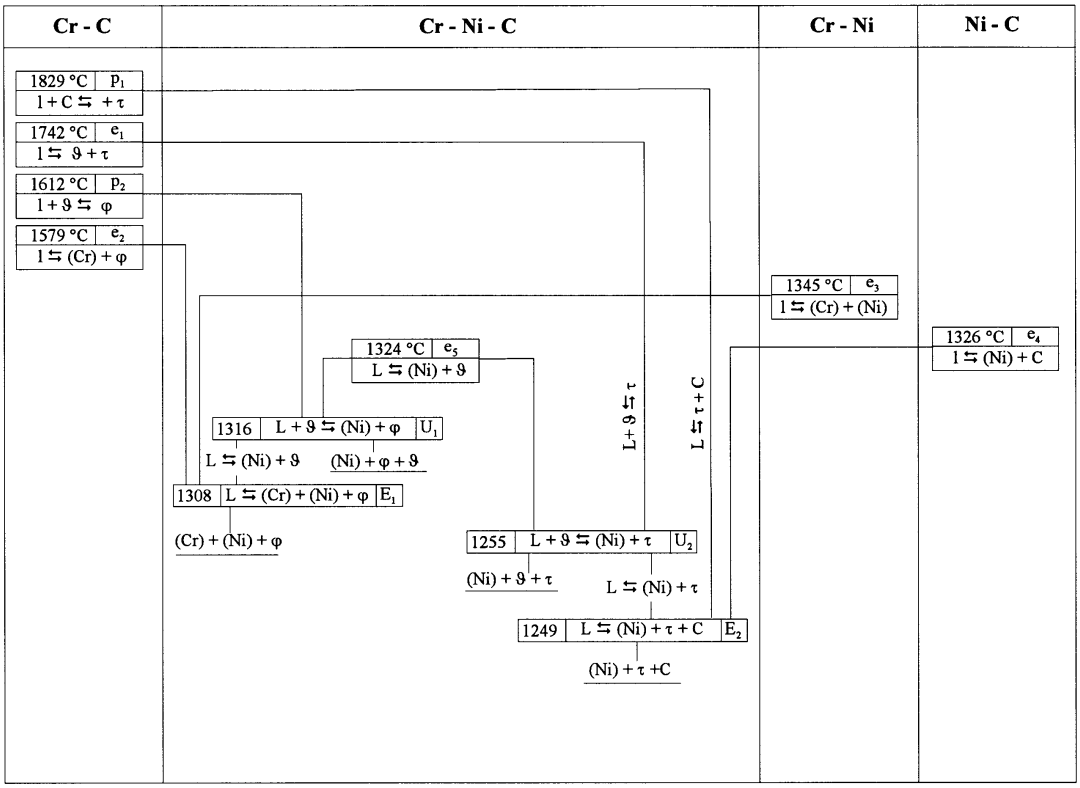

Fig. 4 Reaction scheme for the Cr-Ni-C system at melting (crystallization) of alloys

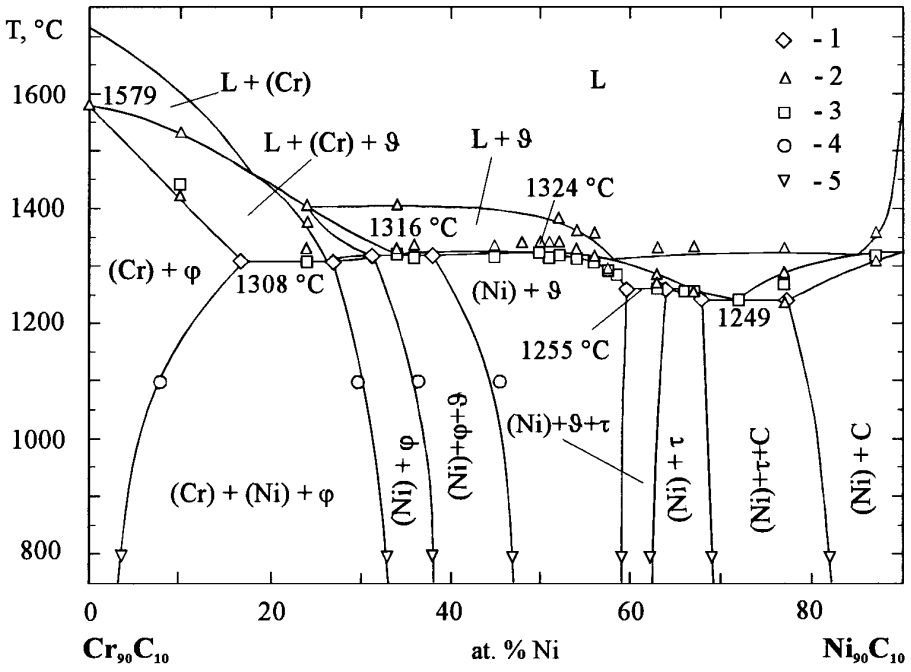

Fig. 5 The vertical section of the Cr-Ni-C phase diagram through the 10 at.% C isoconcentrate. 1, position of phase boundaries on the solidus surface; 2, thermal arrests on differential heating curves; 3, melting temperatures of Pirani-Alterthum method; 4, position of phase boundaries at 1100 °C [71Tel]; 5, at 800 °C [55Kos]

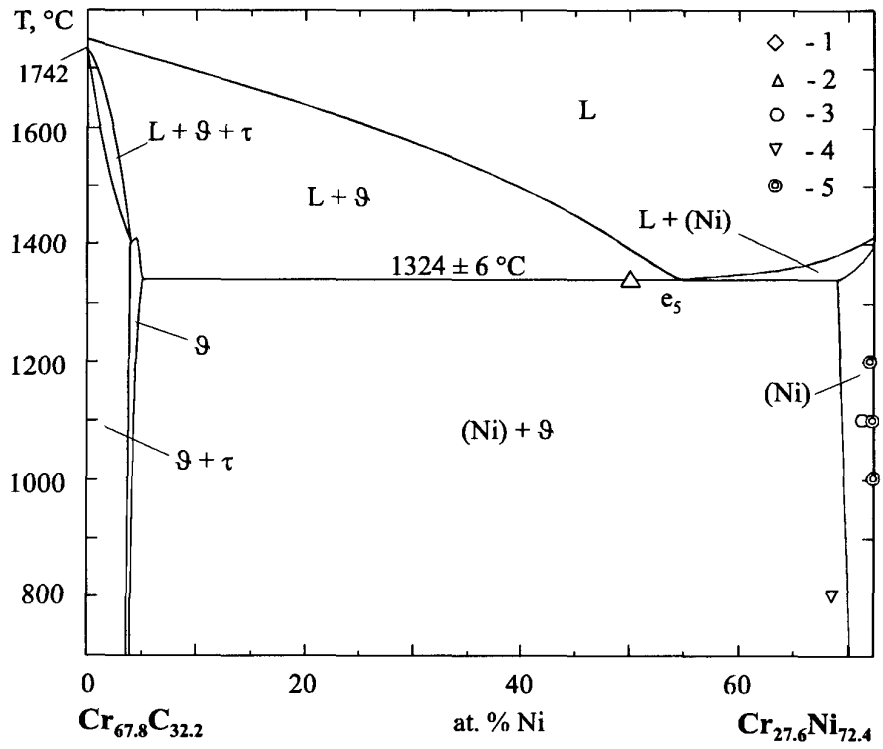

(a)

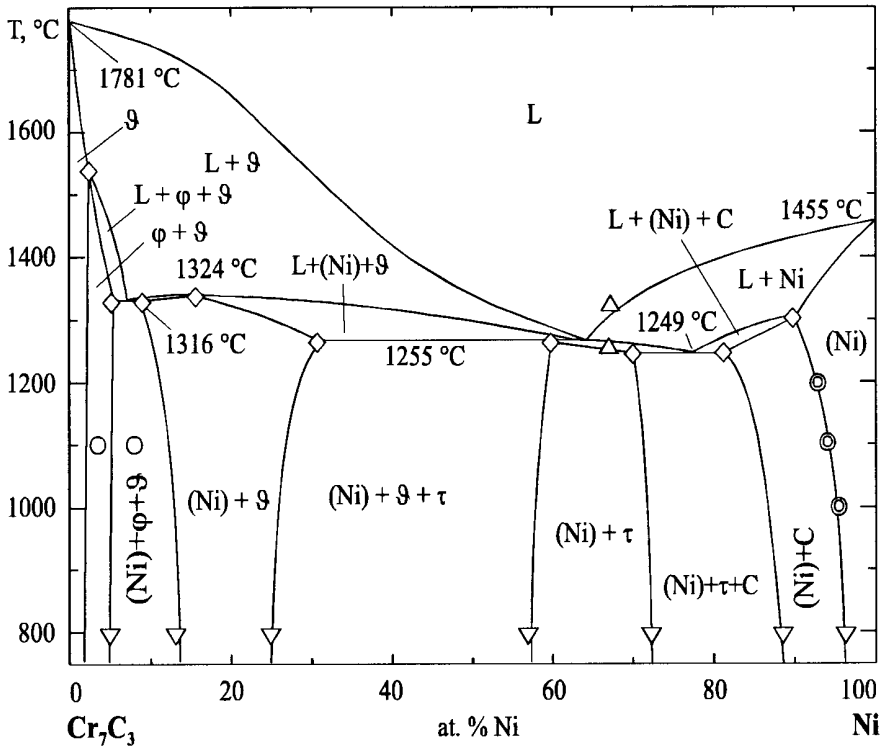

(b)

Fig. 6 The vertical sections of the Cr-Ni-C phase diagram: through the tie line with quasi-binary eutectic (Ni) + (Cr_7C_3) (a) and the nickel-carbides Cr_7C_3 (b), $Cr_{23}C_6$ (c), and Cr_3C_2 (d). 1, position of phase boundaries on the solidus surface; 2, temperatures of phase transformations for alloys of the section; 3, position of phase boundaries at 1100 °C [71Tel]; 4, at 800 °C [55Kos]; 5, [82Tum]. (continued on next page)

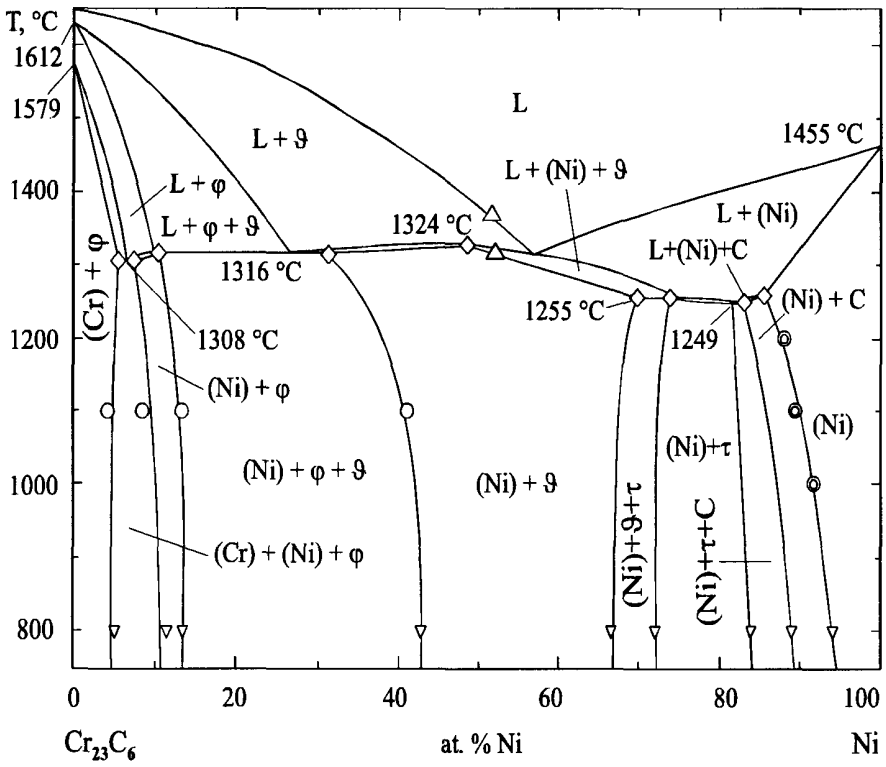

(c)

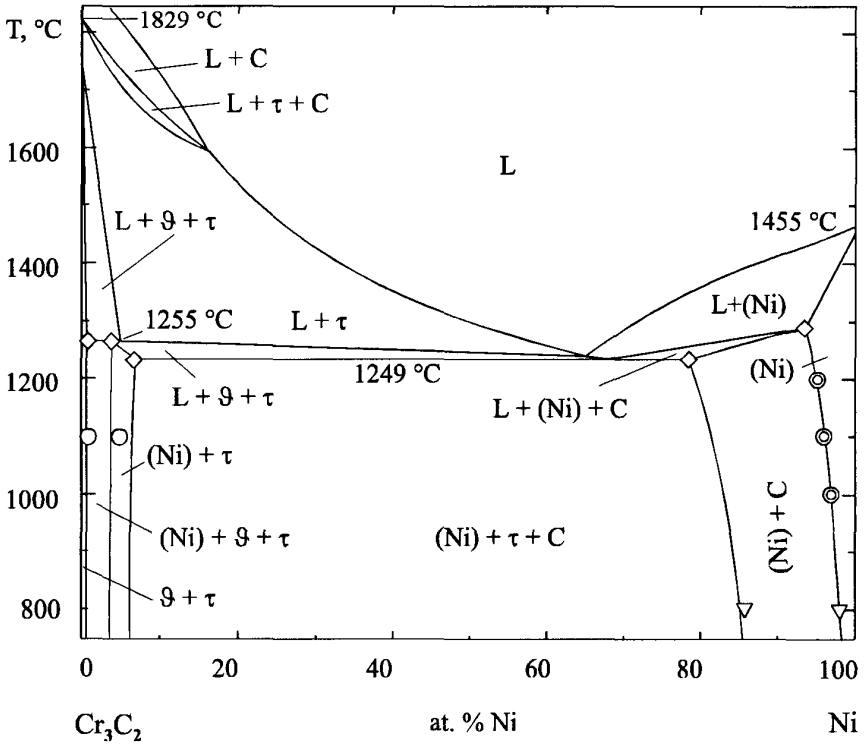

(d)

Fig. 6 cont. The vertical sections of the Cr-Ni-C phase diagram: through the tie line with quasi-binary eutectic (Ni) + (Cr_7C_3) (a) and the nickel-carbides Cr_7C_3 (b), $Cr_{23}C_6$ (c), and Cr_3C_2 (d). 1, position of phase boundaries on the solidus surface; 2, temperatures of phase transformations for alloys of the section; 3, position of phase boundaries at 1100 °C [71Tel]; 4, at 800 °C [55Kos]; 5, [82Tum]

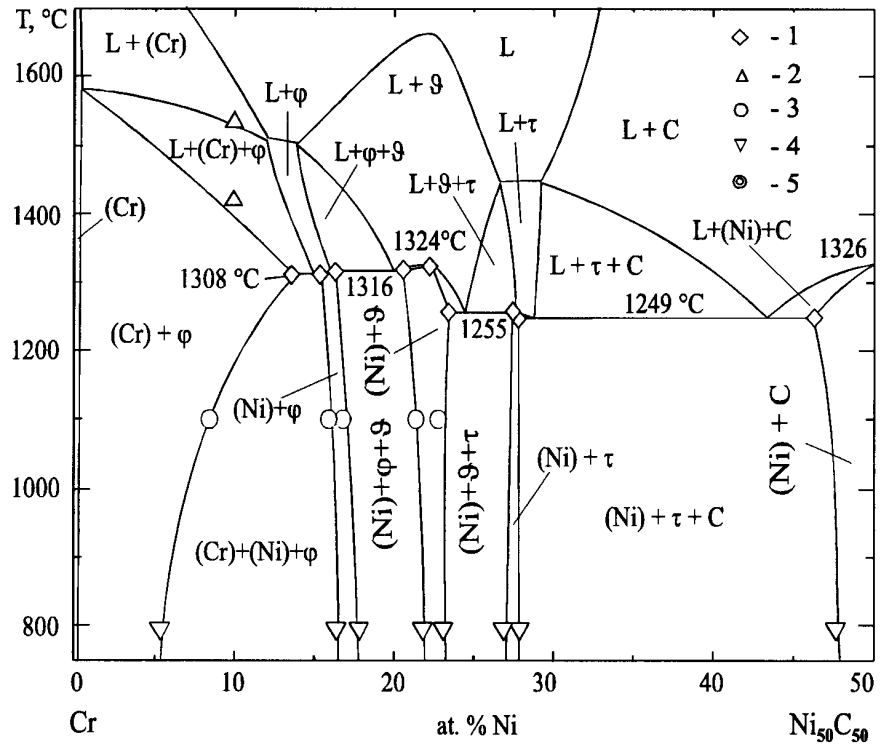

(a)

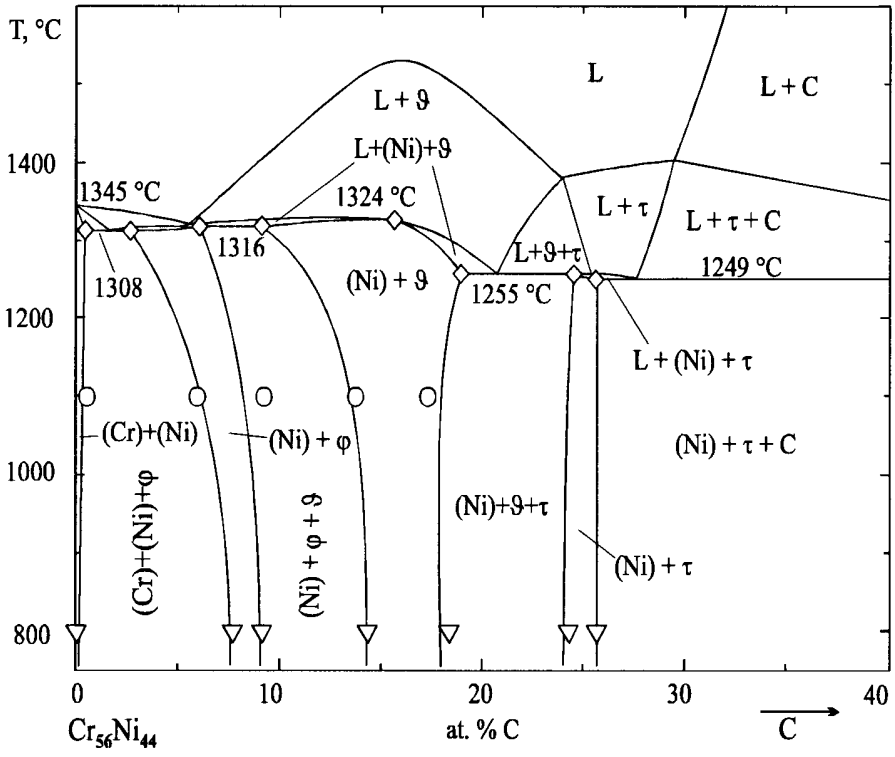

(b)

Fig. 7 The vertical sections of the Cr-Ni-C phase diagram. (a) Cr-$Ni_{50}C_{50}$. (b) C-$Cr_{56}Ni_{44}$ (the composition of (Cr) + (Ni) eutectic). (c) $Cr_{75}C_{25}$-$Ni_{75}C_{25}$. (d) Cr_3C_2-$Cr_{10}Ni_{90}$. 1, position of phase boundaries on the solidus surface; 2, temperatures of phase transformations for alloys of the section; 3, position of phase boundaries at 1100 °C [71Tel], 4, at 800 °C [55Kos]; 5, [82Tum]. (continued on next page)

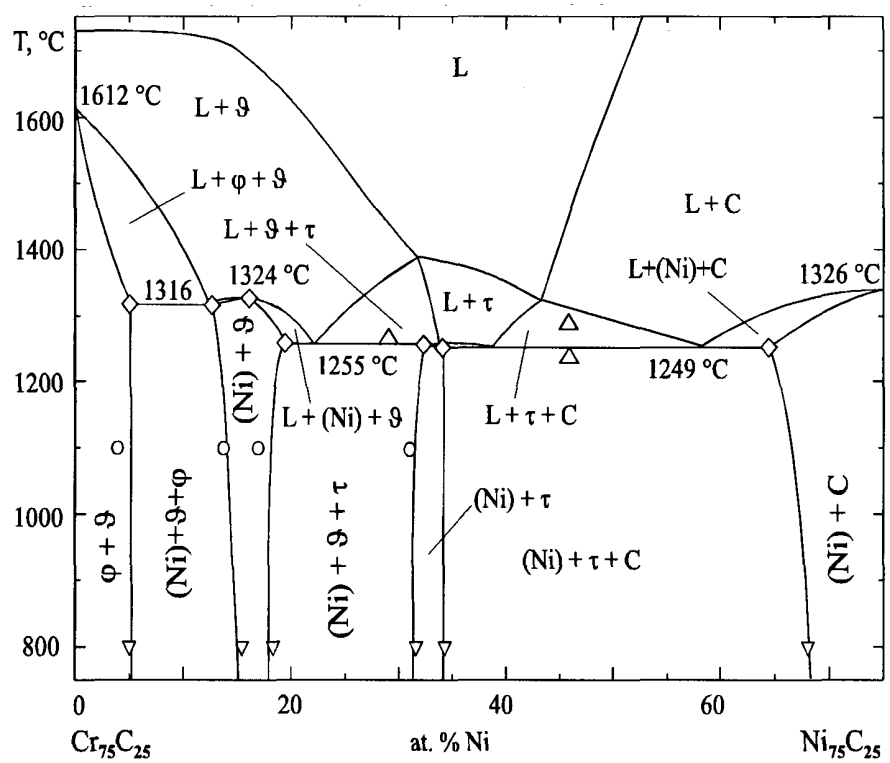

(c)

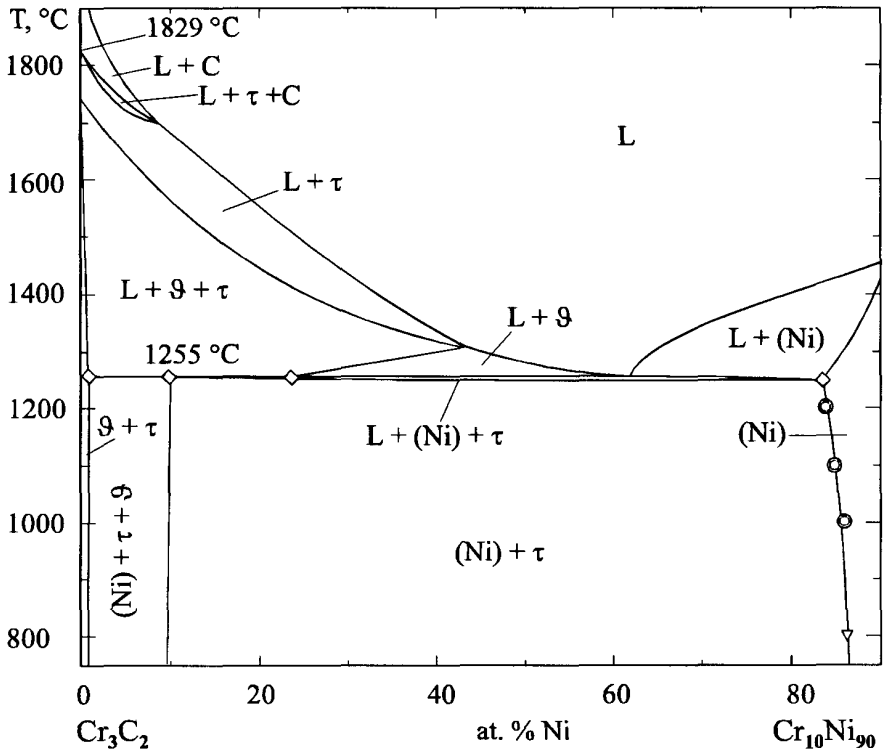

(d)

Fig. 7 cont. The vertical sections of the Cr-Ni-C phase diagram. (a) Cr-$Ni_{50}C_{50}$. (b) C-$Cr_{56}Ni_{44}$ (the composition of (Cr) + (Ni) eutectic). (c) $Cr_{75}C_{25}$-$Ni_{75}C_{25}$. (d) Cr_3C_2-$Cr_{10}Ni_{90}$. 1, position of phase boundaries on the solidus surface; 2, temperatures of phase transformations for alloys of the section; 3, position of phase boundaries at 1100 °C [71Tel], 4, at 800 °C [55Kos]; 5, [82Tum]

Table 5 Phase composition (XRD) and lattice parameters for the as-cast Cr-Ni-C alloys

Composition, at.%					Lattice parameter, pm		
Cr	C	Phase composition	Primary-crystallized phase	Phase	*a*	*b*	*c*
80	10	(Cr) + φ	(Cr)	(Cr)	288.3 ± 0.5	…	…
				φ	1065.1 ± 0.6	…	…
66	10	(Cr) + (Ni) + φ	φ	(Cr)	287.1 ± 0.9	…	…
				(Ni)	359 ± 2	…	…
				φ	1063.0 ± 0.3	…	…
59	18	(Ni) + φ + ϑ	ϑ	(Ni)	358 ± 1	…	…
				φ	1064.0 ± 0.7	…	…
				ϑ	1042.6 ± 0.3	…	452.1 ± 0.3
56	10	(Ni) + φ + ϑ	ϑ	(Ni)	358.0 ± 0.4	…	…
				φ	1064.3 ± 0.9	…	…
				ϑ	(Trace)		
54	10	(Ni) + φ + ϑ	ϑ	(Ni)	354 ± 2	…	…
				φ	1063.7 ± 0.9	…	…
				ϑ	1401 ± 1	…	453.5 ± 0.5
45	10	(Ni) + ϑ	ϑ	(Ni)	358.2 ± 0.3	…	…
				ϑ	1399.4 ± 1.0	…	452.2 ± 1.0
40	10	(Ni) + ϑ	ϑ	(Ni)	355.7 ± 0.4	…	…
				ϑ	1397.3 ± 0.3	…	457 ± 1
38	10	(Ni) + ϑ	ϑ	(Ni)	355.7 ± 0.3	…	…
				ϑ	1401 ± 10	…	451 ± 8
36	10	(Ni) + ϑ	ϑ	(Ni)	356.1 ± 0.4	…	…
				ϑ	1400 ± 1	…	455 ± 1
34	10	(Ni) + ϑ	ϑ	(Ni)	355.4 ± 0.3	…	…
				ϑ	1400.2 ± 0.6	…	454 ± 1
32.5	10	(Ni) + ϑ	ϑ	(Ni)	354.8 ± 0.2	…	…
				ϑ	1402 ± 1	…	452 ± 2
31.5	10	(Ni) + ϑ	(Ni)	(Ni)	355 ± 2	…	…
				ϑ	1399 ± 2	…	455 ± 2
27	10	(Ni) + ϑ	(Ni)	(Ni)	355.3 ± 0.7	…	…
				ϑ	1403 ± 4	…	448 ± 4
46	25	(Ni) + ϑ + τ	ϑ	(Ni)	354 ± 3	…	…
				ϑ	1403.1 ± 0.3	…	449.9 ± 0.4
				τ	555.4 ± 0.3	282.5 ± 0.4	1145 ± 2
24	10	(Ni) + τ	(Ni)	(Ni)	355.92 ± 0.02	…	…
				τ	548 ± 1	297 ± 3	1146.4 ± 0.5
23	10	(Ni) + τ	(Ni)	(Ni)	354.61 ± 0.07	…	…
				τ	552 ± 5	284 ± 1	1146 ± 3
18	10	(Ni) + τ	(Ni)	(Ni)	354.7 ± 0.1	…	…
				τ	553.6 ± 0.3	280.9 ± 0.5	1143 ± 1
13	10	(Ni) + τ	(Ni)	(Ni)	354.44 ± 0.09	…	…
				τ	(Trace)		
29	25	(Ni) + τ	C(a)	(Ni)	354 ± 2	…	…
				τ	552.6 ± 0.2	282.7 ± 0.2	1149.1 ± 0.3
3	10	(Ni)	C(a)	(Ni)	353.49 ± 0.08	…	…
0	90	(Ni)	C(a)	(Ni)	353.23 ± 0.04	…	…
56	0	(Cr) + (Ni)	(Ni)	(Cr)	288.0 ± 0.1	…	…
				(Ni)	359.4 ± 0.6	…	…

(a) Phase was not detected by XRD.

Table 6 Metal atomic ratio for phase (EPMA) of the Cr-Ni-C alloys

Composition, at.%		Phase composition	Alloy state	Structural ingredient	Metal atomic ratio, 100 Cr/(Cr + Ni)
Cr	C				
66	10	(Cr) + (Ni) + φ	Ann.(a)	(Cr)	68.2, 68.8, 67.0
				(Ni)	52.6
				φ	95.0, 95.0
56	10	(Ni) + φ + ν	Ann.	(Ni)	45.5
				φ	93.9
		(Cr) + (Ni) + φ + ν	As-cast	ϑ	98.2
				Eut(b)	60.5
39	10	(Ni) + ϑ	As-cast	(Ni)	32.9, 31.0, 31.2
				ϑ	95.6, 95.36
				Eut	40.9, 41.0
46	25	(Ni) + ϑ + τ	Ann.	(Ni)	17.9, 18.7, 18.3
					18.8, 17.3, 17.1
				ϑ	91.1, 91.4
				τ	98.8, 98.1
27	10	(Ni) + ϑ + τ	Ann.	(Ni)	18.0, 18.4
				ϑ	88.1
29	25	(Ni) + τ + C	Ann.	(Ni)	13.8, 14.1, 14.0
				τ	99.1, 98.6, 99.2, 98.8
29	25	(Ni) + τ + C	As-cast	(Ni)	13.7
				τ	98.9
				Eut	40.2
13	10	(Ni) + τ + C	As-cast	(Ni)	11.2, 11.5, 12.0
				Eut	36.2

(a) Ann., annealed at subsolidus temperature (Table 2). (b) Eut, eutectic structure.

Table 7 Phase compositions and lattice parameters of phases existing in invariant equilibria with liquid in the Cr-Ni-C ternary system

Invariant equilibria	Phase	Composition of phase, at.%			Lattice parameters after present work, pm			Literature data for composition of phase [40Mur]			[55Kos]		
		Cr	Ni	C	*a*	*b*	*c*	Cr	Ni	C	Cr	Ni	C
E_1, 1308 ± 4 °C	L	59.0	38.0	3.0	…	…	…	58.1	40.1	1.8	67.2	28.4	4.3
L ↔ (Cr) + (Ni) + φ	(Cr)	68.0	31.8	0.2	286.5 ± 0.2	…	…	…	…	…	65.8(a)	33.6(a)	0.6(a)
	(Ni)	52.0	47.5	0.5	359.8 ± 0.1	…	…	…	…	…	49.7(a)	49.5(a)	0.8(a)
	φ	75.3	4.0	20.7	1068.7 ± 0.7	…	…	…	…	…	75.5(a)	4.0(a)	20.7(a)
E_2, 1249 ± 9 °C	L	20.0	66.0	14.0	…	…	…	19.1	70.4	10.5	19.4	65.8	14.7
L ↔ (Ni) + τ + C	(Ni)	13.6	83.4	3.0	354.64 ± 0.05	…	…	…	…	…	8.1(a)	89.5(a)	2.4(a)
	τ	59.3	0.7	40.0	553.7 ± 0.5	283.1 ± 0.5	148 ± 2	…	…	…	60.0(a)	0.0(a)	40.0(a)
	C	0	0	100	…	…	…	…	…	…	0.0	0.0	100.0
U_1, 1316 ± 5 °C	L	53.0	42.0	5.0	…	…	…	40.8	56.5	2.7	53.5	41.3	5.3
L + ϑ ↔ (Ni) + φ	ϑ	65.8	4.5	29.7	1042.6 ± 0.3	…	452.1 ± 0.3	…	…	…	65.0(a)	5.0(a)	30.0(a)
	(Ni)	45.2	54.0	0.7	357.8 ± 0.3	…	…	…	…	…	69.1(a)	29.0(a)	1.9(a)
	φ	74.3	5.0	20.7	1064.3 ± 0.3	…	…	…	…	…	75.5(a)	4.0(a)	20.7(a)
U_2, 1255 ± 6 °C	L	26.0	62.0	12.0	…	…	…	23.4	67.4	9.2	26.8	61.2	12.0
L + ϑ ↔ (Ni) + τ	ϑ	64.0	6.0	30.0	1401 ± 2	…	448 ± 2	…	…	…	65.0(a)	5.0(a)	30.0(a)
	(Ni)	17.6	79.9	2.5	355.0 ± 0.3	…	…	…	…	…	15.3(a)	82.2(a)	2.5(a)
	τ	59.4	0.6	40.0	554.4 ± 0.5	283.1 ± 0.6	146 ± 2	…	…	…	60.0(a)	0.0(a)	40.0(a)
e_n, 1324 ± 6 °C	L	37.7	54.3	8.0	…	…	…	…	…	…	32.1	58.4	9.5
L ↔ (Ni) + ϑ	(Ni)	29.5	69.0	1.5	356.1 ± 0.1	…	…	…	…	…	20.0(a)	78.1(a)	1.9(a)
	ϑ	65.0	5.0	30.0	402.4 ± 0.5	…	451.9 ± 0.5	…	…	…	65.0(a)	5.0(a)	30.0(a)

(a) Data were taken from figures given by authors.

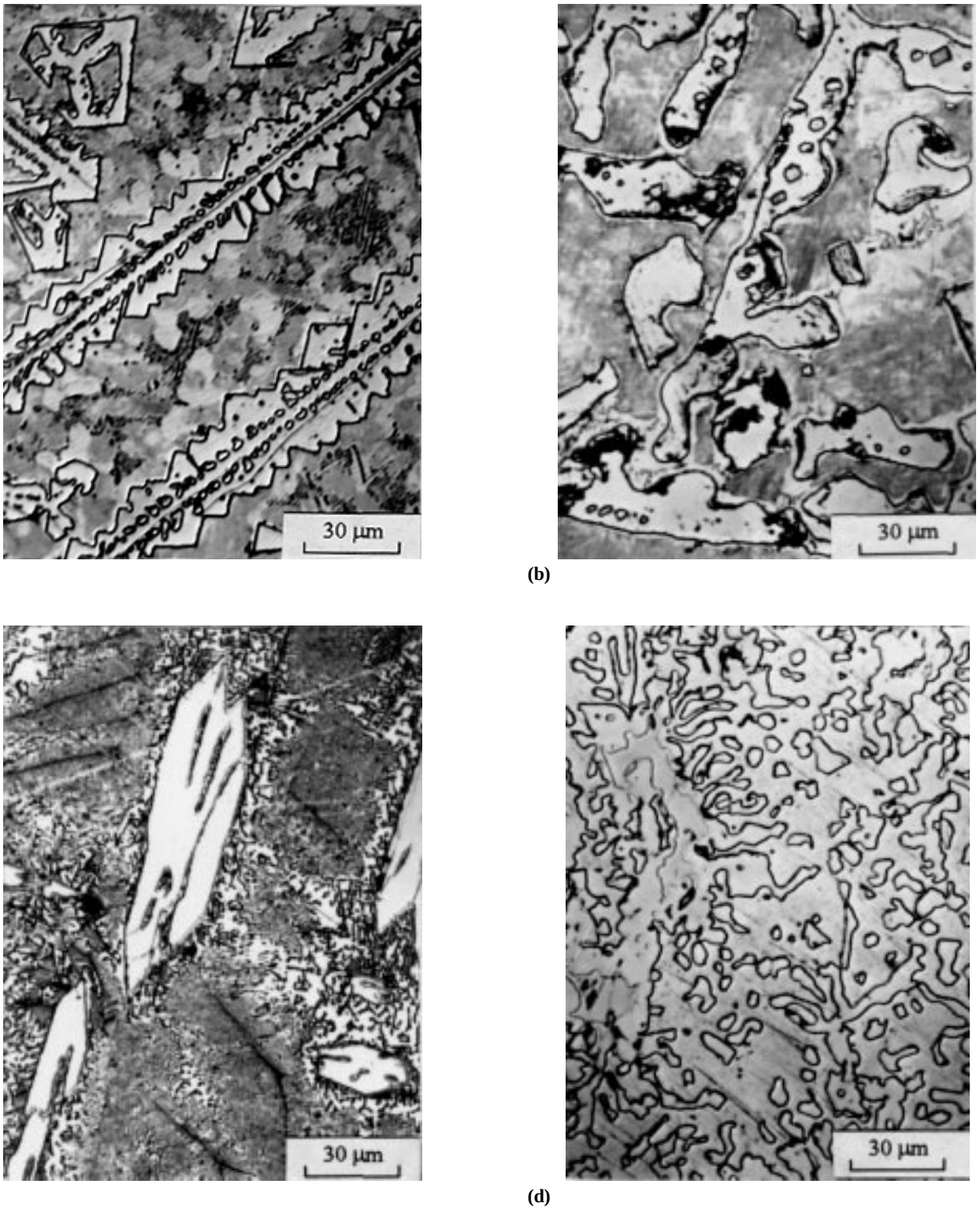

Fig. 8 Microstructures of the Cr-Ni-C alloys, being as-cast and annealed at subsolidus temperatures, which are in the area of invariant four-phase equilibria, 300×. (a) $Cr_{66}Ni_{24}C_{10}$, as-cast; primary-crystallized ($Cr_{23}C_6$), eutectics (Cr) + ($Cr_{23}C_6$) and (Cr) + (Ni) + $Cr_{23}C_6$. (b) The same annealed at 1300 °C for 30 min, (Cr) + (Ni) + ($Cr_{23}C_6$). (c) $Cr_{56}Ni_{34}C_{10}$, as-cast; primary (Cr_7C_3), eutectics (Ni) + (Cr_7C_3) and (Ni) + ($Cr_{23}C_6$). (d) The same annealed at 1300 °C for 30 min, (Ni) + ($Cr_{23}C_6$) + (Cr_7C_3). (e) $Cr_{46}Ni_{29}C_{25}$, as-cast; primary (Cr_7C_3) and eutectic (Ni) + (Cr_7C_3) + (Cr_3C_2). (f) The same annealed at 1230 °C for 30 min, (Ni) + (Cr_7C_3) + (Cr_3C_2). (g) $Cr_{29}Ni_{46}C_{25}$, as-cast, primary graphite, grains of (Cr_3C_2) and eutectic (Ni) + (Cr_3C_2) + C. (h) The same annealed at 1195 °C for 30 min, (Ni) + (Cr_3C_2) + C. (continued on next page)

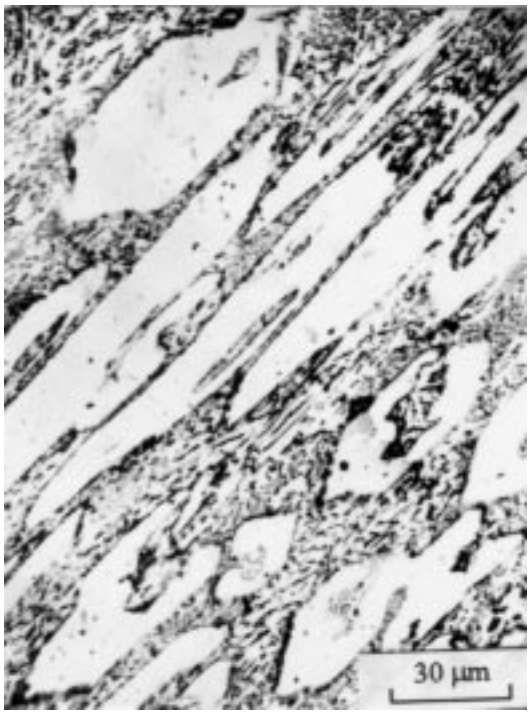

(e)

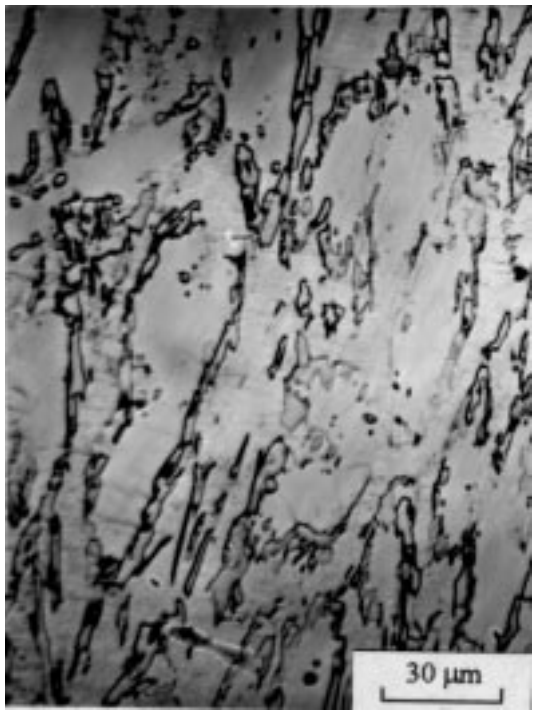

(f)

(g)

(h)

Fig. 8 cont. Microstructures of the Cr-Ni-C alloys, being as-cast and annealed at subsolidus temperatures, which are in the area of invariant four-phase equilibria, 300×. (a) $Cr_{66}Ni_{24}C_{10}$, as-cast; primary-crystallized ($Cr_{23}C_6$), eutectics (Cr) + ($Cr_{23}C_6$) and (Cr) + (Ni) + $Cr_{23}C_6$. (b) The same annealed at 1300 °C for 30 min, (Cr) + (Ni) + ($Cr_{23}C_6$). (c) $Cr_{56}Ni_{34}C_{10}$, as-cast; primary (Cr_7C_3), eutectics (Ni) + (Cr_7C_3) and (Ni) + ($Cr_{23}C_6$). (d) The same annealed at 1300 °C for 30 min, (Ni) + ($Cr_{23}C_6$) + (Cr_7C_3). (e) $Cr_{46}Ni_{29}C_{25}$, as-cast; primary (Cr_7C_3) and eutectic (Ni) + (Cr_7C_3) + (Cr_3C_2). (f) The same annealed at 1230 °C for 30 min, (Ni) + (Cr_7C_3) + (Cr_3C_2). (g) $Cr_{29}Ni_{46}C_{25}$, as-cast, primary graphite, grains of (Cr_3C_2) and eutectic (Ni) + (Cr_3C_2) + C. (h) The same annealed at 1195 °C for 30 min, (Ni) + (Cr_3C_2) + C

The apex coordinates of tie triangles on the solidus surface are presented in Fig. 1 and Table 7. One can see that there is a wide two-phase region (Ni) + (Cr_7C_3). The solidus temperature for the (Ni) + (Cr_7C_3) mixture increases from 1316 °C at the boundary with the three-phase region (Ni) + ($Cr_{23}C_6$) + (Cr_7C_3) to the maximum at 1324 °C and then begins to decrease, reaching the value 1255 °C at the boundary with the three-phase region (Ni) + (Cr_7C_3) + (Cr_3C_2). As this maximum is rather weak (Fig. 5), additional DTA experiments were carried out to detect its exact location. Two two-phase alloys containing 10 at.% C and slightly different concentrations of Ni and Cr were simultaneously placed on the measuring block. One was used as a sample, the other as a standard (Fig. 11a) and vice versa in the second experiment (Fig. 11b). The results of both experiments were in agreement; the more refractory alloy gave the thermal effect of melting at higher temperature. By gradually varying Cr concentration in these experiments, it was found that the maximum melting temperature is characteristic of the $Cr_{40}Ni_{50}C_{10}$ alloy with a value of 1324 ± 6 °C according to the Pirani-Alterthum method (Table 2); this corresponds to the $L_{e_5} \leftrightarrow$ (Ni) + (Cr_7C_3) invariant equilibrium.

The tie line corresponding to this quasi-binary eutectic is located in the section $Cr_{27.6}Ni_{72.4}$-$Cr_{67.8}C_{32.2}$ of the phase diagram (Fig. 6a). In reality, this section is not quasi-binary (pseudobinary) in the classic meaning of this notion because it does not pass through dystectic points of the binary Ni-base and Cr_7C_3 phases of the binary systems. The section Ni-Cr_7C_3 through dystectic points has more complicated structure (Fig. 6b). Furthermore, the section $Cr_{27.6}Ni_{72.4}$-$Cr_{67.8}C_{32.2}$ extrapolates to a composition in the Cr-C binary diagram within the two-phase (Cr_7C_3) + (Cr_3C_2) region. Nevertheless, it seems quite safe to divide the ternary Cr-Ni-C diagram into two partial subsystems, Cr-Cr_7C_3-$(Cr_{0.93}Ni_{0.07})_7C_3$-$Cr_{29.5}Ni_{69}C_{1.5}$-Ni and C-$Cr_7C_3$-$(Cr_{0.93}Ni_{0.07})_7C_3$-$Cr_{29.5}Ni_{69}C_{1.5}$-Ni. The solidus temperatures of both subsystems decrease as the configuration point of the composition moves from the quasi-binary section or from the boundary systems inward. These temperatures reach the minimum values 1308 and 1249

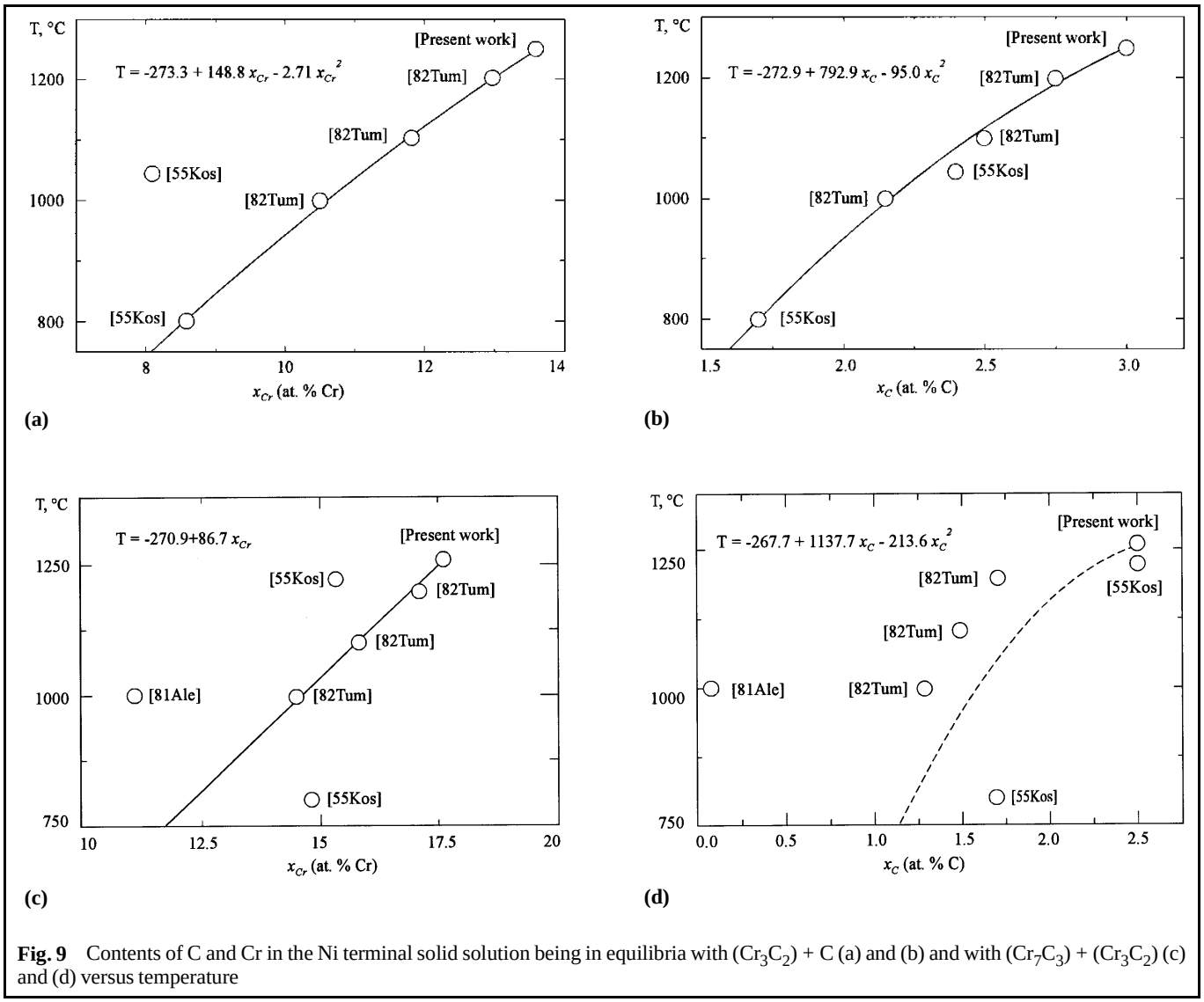

Fig. 9 Contents of C and Cr in the Ni terminal solid solution being in equilibria with (Cr_3C_2) + C (a) and (b) and with (Cr_7C_3) + (Cr_3C_2) (c) and (d) versus temperature

°C in the three-phase regions (Cr) + (Ni) + ($Cr_{23}C_6$) and (Ni) + (Cr_3C_2) + C, as shown in Fig. 4.

4.2 Liquidus Surface

Figure 2 shows the liquidus surface of the Cr-Ni-C phase diagram where the isotherms are given according to the DTA results. The character of phase transformations was also confirmed by studying the microstructures of the as-cast samples. One can see that there are six fields of primary crystallization. They are evidently connected with the six phases found on the solidus surface (Fig. 1). At high C concentration the graphite primary crystallization field is adjusted to the area of equilibria with a gaseous phase and was not investigated in the present work. The saddle point e_5 corresponds to the maximum tem-

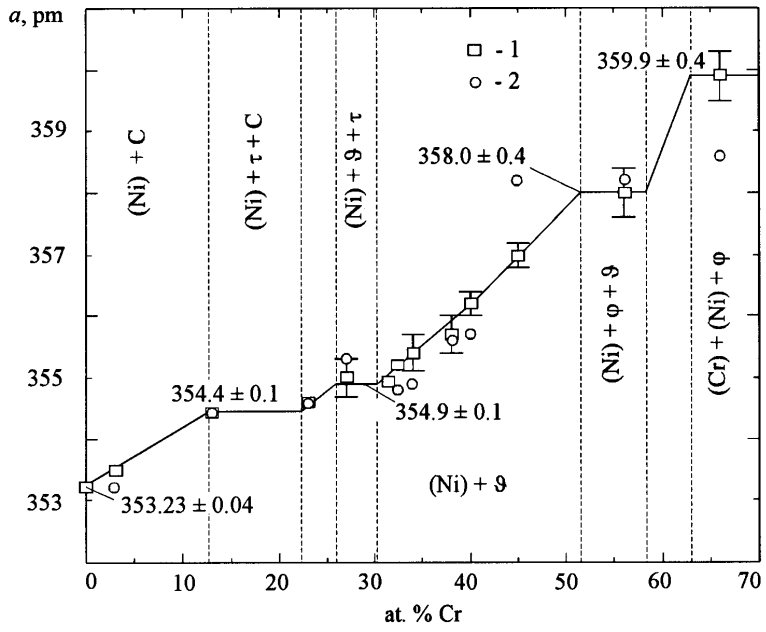

(a)

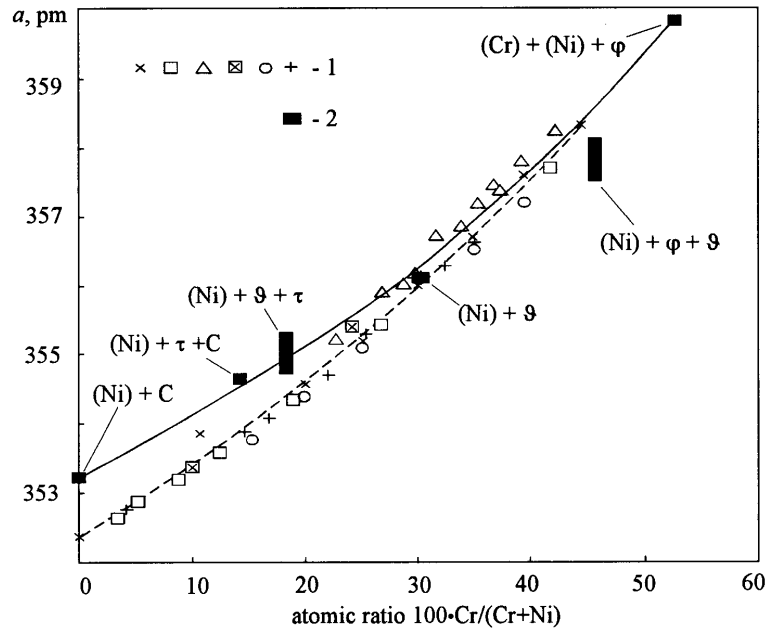

(b)

Fig. 10 Lattice parameters of the Ni solid solution versus composition of alloys of the 10 at.% C section (a) and versus the metal content ratio in the phase (b). 1, alloys annealed at subsolidus temperatures; 2, as-cast alloys; 3, compiled [86Nas] data for binary alloys; 4, the authors' data for ternary alloys (height is based on 95% confidence limit)

perature of the two-phase (Ni) + (Cr_7C_3) ruled solidus surface (Fig. 1).

The micrograph of the as-cast two-phase (Ni) + (Cr_7C_3) alloy $Cr_{40}Ni_{50}C_{10}$ belonging to the quasi-binary section $(Cr_{0.93}Ni_{0.07})_7C_3$-$Cr_{29.5}Ni_{69}C_{1.5}$ is given in Fig. 12(a). Primary-crystallized carbide grains, edged by characteristic rimmed structure, are located in a uniform eutectic matrix formed by crystallization of the liquid at the eutectic temperature 1324 ± 6 °C. In the as-cast alloy $Cr_{32.5}Ni_{57.5}C_{10}$ (Fig. 12b), the amount of primary carbide (Cr_7C_3) is lower, while the eutectic is more coarse grained. This point lies close to the line e_5U_2, which corresponds to the monovariant equilibrium L ↔ (Ni) + (Cr_7C_3). The eutectic structure of the alloy $Cr_{31.5}Ni_{58.5}C_{10}$ in the as-cast state (Fig. 12c) indicates that it belongs to the above line. The as-cast structure of the alloys lying in the region of primary crystallization of (Ni) phase are quite different (Fig. 12d-f) from the foregoing micrographs. For example, one can clearly see the primary crystals of (Ni) and the fine three-phase eutectic (Ni) + (Cr_3C_2) + C mixture in the sample $Cr_{22}Ni_{66}C_{10}$ (Fig. 12f).

The typical structures of the as-cast and annealed alloys belonging to all three phase regions are presented in Fig. 8(a) to (h). Figure 8(a) shows characteristic grains of the primary ($Cr_{23}C_6$) carbide, a conglomerate structure formed during joint congruent crystallization of (Cr) and ($Cr_{23}C_6$), and the three-phase eutectic (Cr) + (Ni) + ($Cr_{23}C_6$) in the as-cast sample of $Cr_{66}Ni_{24}C_{10}$. These three phases were also found out by XRD after annealing at the temperatures 8 to 10 °C below solidus (Fig. 8b). The micrograph of the as-cast alloy $Cr_{56}Ni_{34}C_{10}$ (Fig. 8c) exhibits the grains of the primary-crystallized (Cr_7C_3) carbide and two eutectics: (Ni) + (Cr_7C_3) and (Ni) + ($Cr_{23}C_6$). After annealing for 30 min at 1305 °C (10 °C below solidus), the eutectics become more coarse grain, as can be seen in Fig. 8(d). Three-phase structure (Ni) + (Cr_7C_3) + (Cr_3C_2) can be seen in the micrographs of both as-cast and annealed samples of the $Cr_{46}Ni_{29}C_{25}$ alloy (Fig. 8e and f). Primary grains of (Cr_7C_3) are distributed in the eutectic matrix (Ni) + (Cr_7C_3) + (Cr_3C_2). The microstructure of the as-cast alloy $Cr_{29}Ni_{46}C_{25}$ located in the region of graphite primary crystallization is presented in Fig. 8(g). One can see black graphite grains and well-formed grains (Cr_3C_2), distributed in the eutectic matrix (Ni) + (Cr_3C_2) + C. Though the eutectic structure of (Ni) + (Cr_3C_2) + C was observed in several alloys (Fig. 8g, 12f), it was not possible to determine the eutectic composition exactly. Composition of this eutectic, according to [40Mur], corresponds to $Cr_{19.1}Ni_{70}C_{10.9}$ and, according to [55Kos], corresponds to $Cr_{20}Ni_{65}C_{15}$. However, it can be seen from the experimentally constructed vertical section corresponding to the 10 at.% C isoconcentrate (Fig. 5) that the difference between solidus and liquidus temperatures for the three-phase (Ni) + (Cr_3C_2) + C region is about 100 °C. This fact contradicts the eutectic composition reported by [40Mur]. For this reason, in the present work the eutectic composition was accepted according to the recommendation of [55Kos].

Table 8 Comparison of temperatures for invariant equilibria of the Cr-Ni-C ternary system given by different authors

Invariant equilibria	Temperature, °C		
	$t_{real} \pm \Delta_{tot}$(a)	[40Mur](b)	[55Kos](b)
L ↔ (Ni) + τ + C	1249 ± 9	1240	1045
L + ϑ ↔ (Ni) + τ	1255 ± 6	1260	~1220
L ↔ φ + (Cr) + (Ni)	1308 ± 4	1305	1270
L + ϑ ↔ (Ni) + φ	1316 ± 5	1315	~1280
L ↔ (Ni) + ϑ	1324 ± 6	…	1305

(a) Authors' data. (b) Correction for IPTS used by authors was not carried in.

The temperatures of the invariant equilibria given by different authors are compared in Table 8. Good agreement can be seen between the present results and the data of [40Mur]. The temperatures recommended by [55Kos] are 20 to 200 °C lower. In contrast to the temperature results, the compositions of the phases involved in all invariant equilibria (Table 7) found in the present investigation are closer to the data of [55Kos].

4.3 Vertical Sections

Three of the most interesting vertical (polythermal) sections of the Cr-Ni-C phase diagram, resulting from the present

Table 9 Composition of phases coexisting in three-phase equilibria at selected temperatures

Three-phase region	Phase	Composition of phase at 800 °C, at.%			Composition of phase at 1000 °C, at.%			Composition of phase at 1100 °C, at.%			Composition of phase at 1200 °C, at.%		
		Cr	Ni	C	Cr	Ni	C	Cr	Ni	C	Cr	Ni	C
(Ni) + τ + C	(Ni)	8.6	89.7	1.7	10.6	87.2	2.2	11.8	85.7	2.5	13.0	84.2	2.8
	τ	59.5	0.5	40	59.4	0.6	40	59.4	0.6	40	59.3	0.7	40
	C	0	0	100	0	0	100	0	0	100	0	0	100
(Ni) + ϑ + τ	(Ni)	12.4	86.4	1.2	14.7	83.7	1.6	15.8	82.4	1.8	17.0	80.8	2.2
	ϑ	64.0	6.0	30.0	64.0	6.0	30.0	64.0	6.0	30.0	64.0	6.0	30.0
	τ	59.6	0.4	40	59.5	0.5	40	59.5	0.5	40	59.4	0.6	40
(Ni) + φ + ϑ	(Ni)	30.3	69.2	0.5	36.0	63.4	0.6	38.8	60.6	0.6	41.6	57.7	0.7
	φ	74.3	5.0	20.7	74.3	5.0	20.7	74.3	5.0	20.7	74.3	5.0	20.7
	ϑ	65.6	4.5	29.9	65.7	4.5	29.8	65.7	4.5	29.8	65.8	4.5	29.7
(Cr) + (Ni) + φ	(Cr)	97.6	2.2	0.2	94.6	5.2	0.2	89.2	10.6	0.2	72.7	27.1	0.2
	(Ni)	38.4	61.3	0.3	44.1	55.5	0.4	46.3	53.3	0.4	49.0	50.5	0.5
	φ	75.3	4.0	20.7	75.3	4.0	20.7	75.3	4.0	20.7	75.3	4.0	20.7

investigation of the melting range and a critical analysis of the available data, are given in Fig. 5 to 7. The authors consider their data for solidus temperatures to be highly reliable because the state of equilibrium was undoubtedly reached during annealing at subsolidus temperatures, and this fact was confirmed by agreement among the results obtained by different experimental methods. The 800 °C isothermal section proposed by [55Kos] is in reasonable agreement with their solidus surface, so the Köster-Kabermann section was used for construction of all polythermal sections. Results of [71Tel] seem to be reliable only for the Cr corner of the diagram where precipitation of the ($Cr_{23}C_6$) carbide phase occurs. In the other parts of diagram, the data reported by [71Tel] diverge from the common picture. The information obtained in [82Tum] was also used for description of the solvus surface of the Ni-base solid solution while keeping in mind the hypothesis about absence of solubility at 0 K.

The vertical section $Cr_{90}C_{10}$-$Ni_{90}C_{10}$ is given in Fig. 5 and includes present experimental results for 19 alloys that belong to this section. This section is seen to intersect all invariant planes of the Cr-Ni-C system. It demonstrates clearly the complexity of phase relationships in this system. The shadow (weak) maximum of the ruled (Ni) + (Cr_7C_3) solidus surface discussed earlier is clearly seen in Fig. 6(b) and (c) and 7(a) to (c), as well as in Fig. 5. The related maximum in the liquidus surface is also seen in Fig. 7(a) and (b).

The $Cr_{67.8}C_{32.2}$-$Cr_{27.6}Ni_{72.4}$ vertical section is the most simple (Fig. 6a). The quasi-binary eutectic $L_{e_5} \leftrightarrow$ (Ni) + (Cr_7C_3) at 1324 °C represents the degenerated tie L + (Ni) + ϑ triangle. This section crosses the region of $(Cr,Ni)_7C_3$ carbide stability near the composition of maximal saturation of this phase with Ni. In comparison, the polythermal section Ni-Cr_7C_3, as well as Ni-$Cr_{23}C_6$ and Ni-Cr_3C_2, intersects a number of isothermal planes of four four-phase invariant equilibria and is characterized by a more complicated constitution (Fig. 6b-d).

Vertical sections Ni-Cr_3C_2 and $Ni_{90}Cr_{10}$-Cr_3C_2 (Fig. 6d, 7d) are interesting because they include the area of compositions of industrial materials on the (Cr_3C_2) + Ni base. It follows from the Fig. 6(d) if these materials are prepared from pure Ni and stoichiometric Cr_3C_2, they should be three phase and contain graphite together with (Ni) and (Cr_3C_2) over a wide composition range. It is possible to avoid formation of graphite replacing pure Ni by Ni-Cr alloy containing 9 to 15 at.% Cr (Fig. 7d). Similar results can be achieved by using a Cr_3C_2 + Cr_7C_3 mixture instead of stoichiometric Cr_3C_2 carbide. In the last case, the final phase composition of the material depends on the ratio of the carbide ingredients and Ni in the starting mixture, as can be seen from the Cr-Ni-C phase diagram (Fig. 1). This problem was discussed in detail by [97Bon], who recommended sintering the desired material as a mixture of the carbides containing 13.2 mass% C with 15 mass% Ni.

4.4 Isothermal Sections

A number of isothermal sections of Cr-Ni-C were constructed by the authors through use of a detailed treatment of all available data; results are given in Fig. 13(a) to (d) and Table 9. Temperature dependencies of Cr and C solubilities in Ni for tie triangles (Ni)-(Cr_3C_2)-C and (Ni)-(Cr_7C_3)-(Cr_7C_3) are given in Fig. 9. The assessment shows reasonable correspondence of the authors' data at solidus temperatures to data at 800 °C [55Kos], at 1000 to 1200 °C [82Tum], and partially to data at 1100 °C [71Tel].

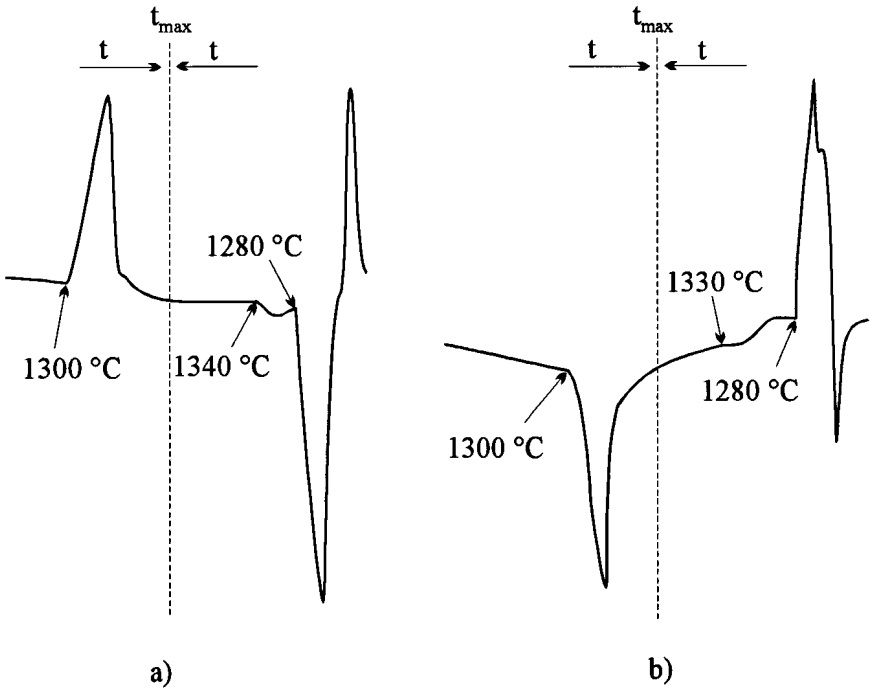

Fig. 11 Differential heating curves of the comparative DTA experiments for alloys of (Ni) + (Cr_7C_3) region. (a) The alloy $Cr_{40}Ni_{50}C_{10}$ is in the place of test sample, and $Cr_{42}Ni_{48}C_{10}$ is in the place of reference sample. (b) The alloy places are exchanged.

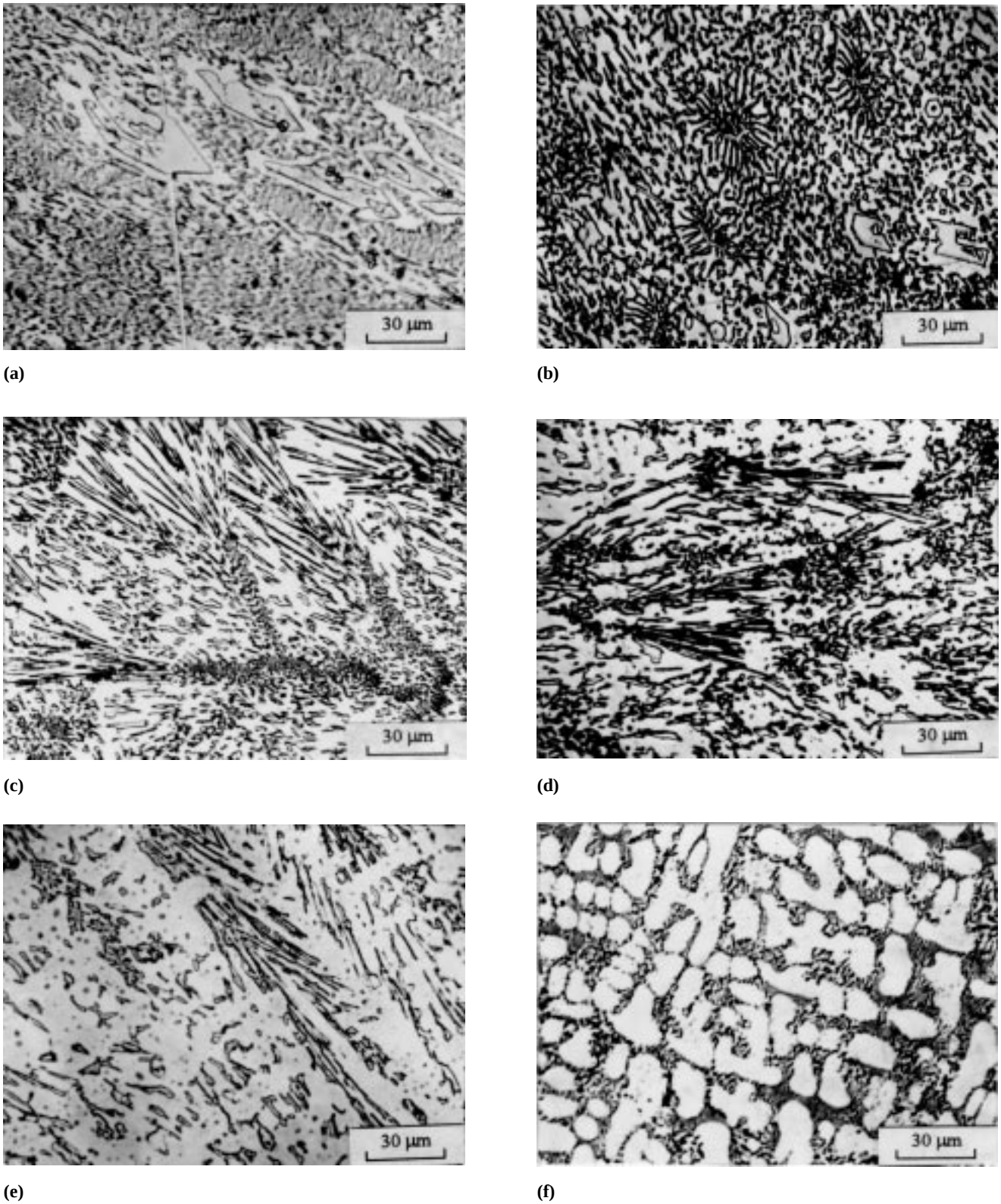

Fig. 12 Microstructures of the Cr-Ni-C as-cast alloys of 10 at.% C section, 300×. (a) $Cr_{40}Ni_{50}C_{10}$; primary-crystallized (Cr_7C_3) and quasi-binary eutectic (Ni) + (Cr_7C_3). (b) $Cr_{32.5}Ni_{57.5}C_{10}$; primary (Cr_7C_3) and eutectic (Ni) + (Cr_7C_3). (c) $Cr_{31.5}Ni_{58.5}C_{10}$; eutectic (Ni) + (Cr_7C_3). (d) $Cr_{27}Ni_{63}C_{10}$; primary (Ni) and eutectic (Ni) + (Cr_3C_2). (e) $Cr_{24}Ni_{66}C_{10}$; primary (Ni) and eutectic (Ni) + (Cr_3C_2). (f) $Cr_{23}Ni_{67}C_{10}$; primary (Ni) and eutectic (Ni) + (Cr_3C_2) + C

The isothermal section at 800 °C (Fig. 13d) is close to that reported in [55Kos] except for the existence of the region of Cr-base solid solution, solubilities of C in metallic phases, and position of carbide apices of tie triangles. The isothermal sections for 1000, 1100, and 1200 °C are more divergent from literature diagrams. [82Tum] and [81Ale] reported nothing about the solubility of Ni in chromium carbides and positions of tie triangles involving equilibria with ($Cr_{23}C_6$) carbide. The main difference from the isothermal section of [71Tel] for 1100 °C are in the positions of two tie triangle apices in the Ni-rich part of the diagram.

4.5 The Common Characteristic of Phase Equilibria in the System

There are no ternary compounds in the Cr-Ni-C system. The Ni-base phase forms equilibria with all others, including the

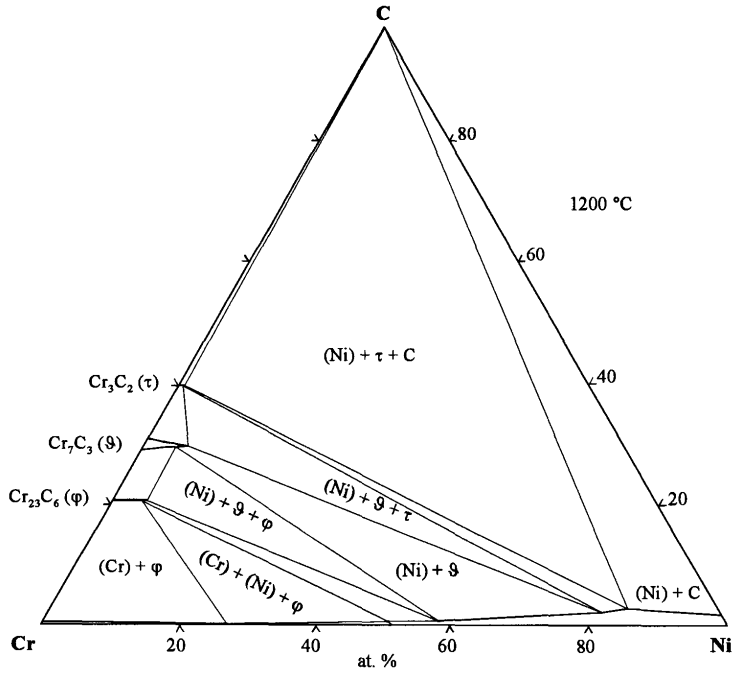

(a)

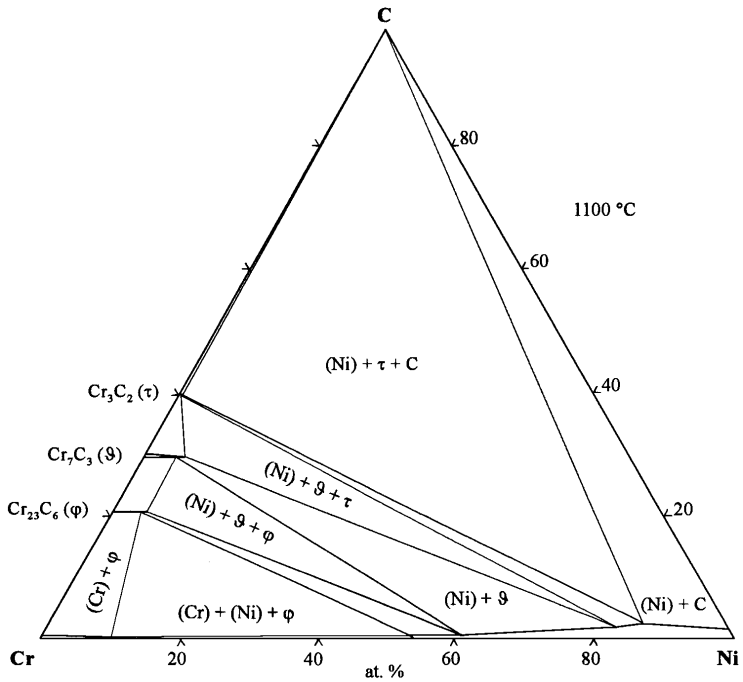

(b)

Fig. 13 Isothermal sections of the Cr-Ni-C phase diagram at: (a) 1200, (b) 1100, (c) 1000, and (d) 800 °C. (continued on next page)

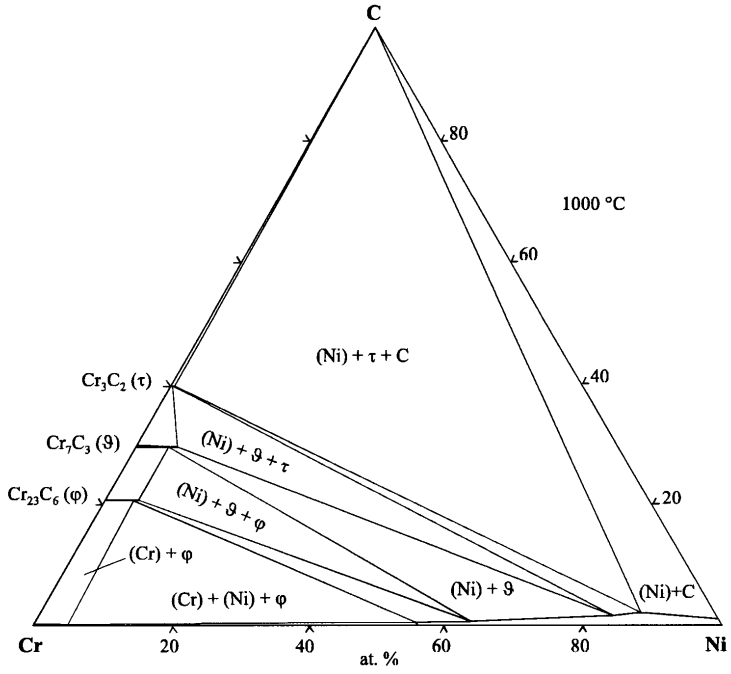

(c)

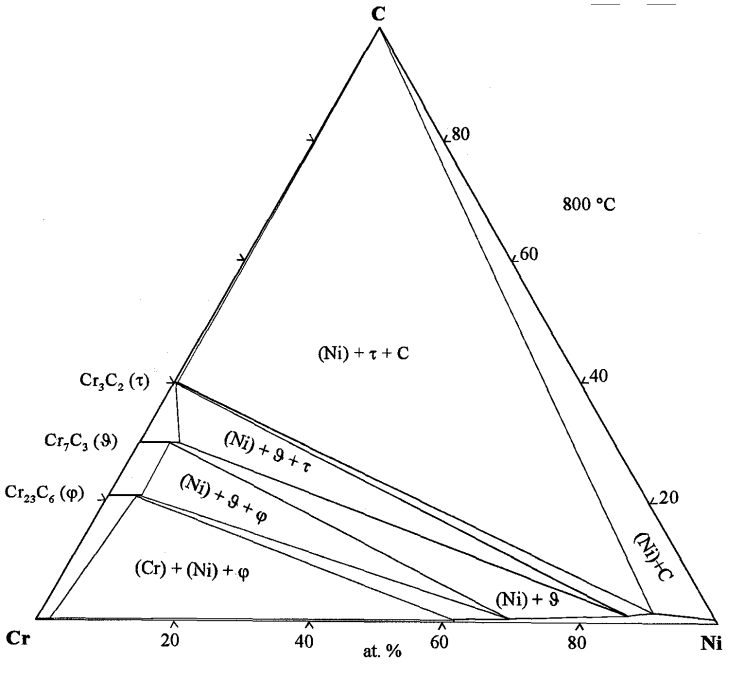

(d)

Fig. 13 cont. Isothermal sections of the Cr-Ni-C phase diagram at: (a) 1200, (b) 1100, (c) 1000, and (d) 800 °C

quasi-binary eutectic $L_{e_5} \leftrightarrow (Ni) + (Cr_7C_3)$ with the (Cr_7C_3) solid solution based on the congruently melting Cr_7C_3 carbide. Due to the latter, there is the possibility of dividing the Cr-Ni-C ternary system into two partial systems: Cr-Cr_7C_3-$(Cr_{0.93}Ni_{0.07})_7C_3$-$Cr_{29.5}Ni_{69}C_{1.5}$-Ni and C-$Cr_7C_3$-$(Cr_{0.93}Ni_{0.07})_7C_3$-$Cr_{29.5}Ni_{69}C_{1.5}$-Ni. All invariant transformations in the ternary system proceed in the narrow temperature range (1249 to 1324 °C). These temperatures are lower than in related binary systems. The projection of solidus surface and isothermal sections for all investigated temperatures (down to 800 °C) differ only in widths of homogeneity regions for (Ni) and (Cr) solid solutions with attendant shifts of related phase boundaries.

References

23Pir: M. Pirani and H. Alterthum, *Z. Elektrochem.*, Vol 29 (No. 1-2), 1923, p 5-8 (in German). (Experimental)

***40Mur:** T. Murakami, S. Takeda, K. Mutsuzaki, and T. Murase, *J. Jpn. Inst. Met.*, Vol 4 (No. 7), 1940, p 189-198 (in Japanese); cited after [95Vil]. (Experimental; #)

51Hes: J.B. Hess, *Acta Crystallogr.*, Vol 4 (No. 3), 1951, p 209-215. (Experimental)

***55Kos:** W. Köster and S. Kabermann, *Arch. Eisenhüttenwes.*, Vol 26 (No. 10), 1955, p 627-630 (in German). (Experimental; #)

64Lis: V.Ye. Listovnichiy, *Inzh.-Fiz. Zh.*, Vol 7 (No. 11), 1964, p 32-35 (in Russian). (Experimental)

65Yer: V.N. Yeremenko and V.Ye. Listovnichiy, *Teplofiz. Vys. Temp.*, Vol 3 (No. 2), 1965, p 234-237 (in Russian). (Experimental)

67Rud: E. Rudy and J. Progulski, *Planseeber. Pulvermetall.*, Vol 15 (No. 1), 1967, p 13-45. (Experimental)

69Rud: E. Rudy, "Ternary Phase Equilibria in Transition Metal-Boron- Carbon-Silicon Systems. Part V. Compendium of Phase Diagram Data," AFML-TR-65-2, Air Force Materials Laboratory, 1969. (Review; #)

71Koc: Yu.A. Kocherzhynskij, Ye.A. Shishkin, and V.I. Vasilenko, *Phase Diagrams of Metal Systems*, Nauka, Moskow, 1971, p 245-249 (in Russian). (Experimental)

71Tel: V.S. Telegus and Yu.B. Kuz'ma, *Visn. Lviv. Derzh. Univer., Ser. Chimichna*, Vol 12, 1971, p 28-33 (in Ukrainian) (Experimental; #)

74Lob: K. Löbl, H. Tuma, and M. Ciznerová, *Mém. Sci. Rev. Métall.*, Vol 71 (No. 5), 1974, p 271-279 (in French). (Experimental)

75Tum: H. Tuma and M. Ciznerová, *Kovové Mater.*, Vol 13 (No. 6), 1975, p 779-782 (in Czech). (Experimental)

77Pou:J.J. Poubeau, "Solubility of Carbon in Chromium and Precipitation of Carbides in the Metal," Engineering Doctorate Thesis, University of Paris, 1977 (in French). (Experimental; #)

81Ale: V.I. Alekseev, I.V. Degtyarova, and G.A. Levshin, *Phase Diagrams of Metal Systems*, N.V. Ageev et al., Ed., Nauka, Moskow, 1981, p 91-98 (in Russian). (Experimental; #)

81Guz: L.S. Guzey, V.N. Kuznetsov, and Ye.M. Sokolovskaya, *Phase Diagrams of Metal Systems*, N.V. Ageev et al., Ed., Nauka, Moskow, 1981, p 103-106 (in Russian). (Calculation; #)

82Tum: H. Tuma and M. Ciznerová, *Kovové Mater.*, Vol 20 (No. 4), 1982, p 426-443 (in Czech); TR: *Met. Mater.*, Vol 20 (No. 4), 1982, p 450-467. (Experimental; #)

85Pou: J. J. Poubeau and J. Bigot, *Acta Metall.*, Vol 33 (No. 6), 1985, p 1137-1141 (in French). (Experimental; #)

85Nas: P. Nash, *Bull. Alloy Phase Diagrams*, Vol 7 (No. 5), 1985, p 466-476, 507-508. (Review; #)

87Yer: V.N. Yeremenko, T.Ya. Velikanova, and A.A. Bondar, *Poroshk. Metall.*, (No. 5), 1987, p 70-76 (in Russian); TR: *Sov. Powder Metall. Met. Ceram.*, Vol 26 (No. 5), 1967, p 409-414. (Experimental; #)

89Sin: M.F. Singleton and P. Nash, *Bull. Alloy Phase Diagrams*, Vol 10 (No. 2), 1989, p 121-126. (Review; #)

90Kaj:M. Kajihara and M. Hillert, *Metall. Trans. A*, Vol 21A (No. 10), 1990, p 2777-2787. (Calculation; #)

90Mas: T.B. Massalski, P.R. Subramanian, H. Okamoto, and L. Kacprzak, Ed., *Binary Alloy Phase Diagrams*, 2nd ed., Vol 1-3, ASM International, 1990. (Review; #)

90Ven: M. Venkatraman and J.P. Neumann, *Bull. Alloy Phase Diagrams*, Vol 11 (No. 2), 1990, p 152-159 (Review; #)

91Nas: P. Nash, *Phase Diagrams of Binary Nickel Alloys*, ASM International, 1991. (Review; #)

91Vil: P. Villars and L.D. Calvert, Ed., *Pearson's Handbook of Crystallographic Data for Intermetallic Phases*, 2nd ed., Vol 1-4, ASM International, 1991. (Review; #)

93Bon: A.A. Bondar, V.A. Maslyuk, and A.V. Grytsiv, *Phase Equilibria, Phase Stability and Metastable States in Metal Systems*, I.N. Frantsevich Institute for Problems of Materials Science of National Academy of Science of Ukraine, Kiev, 1993, p 148-153. (Properties; #)

95Vil: P. Villars, A. Prince, and H. Okamoto, Ed., *Handbook of Ternary Alloy Phase Diagrams*, ASM International/Materials Information Society, 1995. (Review; #)

97Bon: A.A. Bondar, V.A. Maslyuk, T.Ya. Velikanova, and A.V. Grytsiv, *Poroshk. Metall.*, (No. 5/6), 1997, p 13-24 (in Russian); TR: *Powder Metall. Met. Ceram.*, Vol 36 (No. 5/6), 1997. (Properties; #)

*Indicates key paper.

#Indicates presence of a phase diagram.